

Enhancing Synthetic Rating Curve Development Through Empirical Roughness Built for Hydrofabric Datasets

J. Michael Johnson¹, Damilola Eyelade¹, Justin Singh-Mohudpur¹, Arash Modaresi Rad¹, James Coll¹, Ryan Spies¹, and Lilit Yeghiazarian²

¹Lynker

²University of Cincinnati

March 15, 2024

Abstract

Rating curves are commonly developed through direct observation, open channel flow models, or mechanical methods, each relying on in-situ measurement. As part of a U.S. effort to provide high resolution, continental scale, flood mapping, synthetic rating curves (SRCs) were developed across the National Hydrography Dataset (NHDPlusV2) to translate flows, like those generated by the NOAA National Water Model, into river depths. This approach uses Digital Elevation Models (DEM) to define the necessary cross-sectional properties for Manning's equation. A significant limitation, alongside an opportunity for broad improvement, has been assigning suitable roughness without local information. We applied the DEM based methodology to generate SRCs at 7,270 locations with known USGS rating curves, and calibrated roughness to minimize the error between predicted and observed flow. Subsequently, we tested several approaches based on land cover, stream order, and the hydrographic network to estimate the optimized values in a manner that can be extended to ungauged catchments. Among these, a predictive Machine Learning (ML) model based on the NHDPlusV2 network attributes demonstrated superior ability to estimate the optimized roughness with a Spearman correlation of 0.89. Sensitivity analysis showed improving accuracy of DEM and roughness is crucial for accurate estimation of the lower and mid/upper parts of SRC, respectively. Finally, we applied the predictive model over the NHDPlusV2, generating reach-level roughness estimates that can directly support national flood mapping efforts. The method is generalizable to any hydrofabric network that contains topology, however the generated values are dependent on the DEM and hydrofabric used.

1 **Enhancing Synthetic Rating Curve Development Through Empirical Roughness**
2 **Built for Hydrofabric Datasets**
3

4 **J. Michael Johnson^{1,2,3}, Damilola Eyelade^{1,2,3}, Justin Singh-Mohudpur^{1,2,3}, Arash Modaresi**
5 **Rad^{1,3}, James Coll^{1,3}, Ryan Spies^{1,3}, Lilit Yeghiazarian⁴**

6 ¹ Lynker, Fort Collins Colorado USA.

7 ² Department of Geography, University of California, Santa Barbara, California, USA.

8 ³ NOAA NWS Office of Water Prediction

9 ⁴University of Cincinnati
10

11 Corresponding author: J Michael Johnson (jjohnson@lynker.com)

12 **Key Points:**

- 13 • We established synthetic rating curves (SRC) at 7,270 gaged locations and calibrated roughness
14 to minimize error in predicted streamflow.
- 15 • A predictive model based on hydrofabric network properties was built to estimate roughness to
16 support SRC creation in ungauged basins.
- 17 • These predictions achieved a correlation of 0.89 but are likely dependent on the resolution of the
18 DEM and hydrofabric used.

19 **Abstract**

20 Rating curves are commonly developed through direct observation, open channel flow models,
21 or mechanical methods, each relying on in-situ measurement. As part of a U.S. effort to provide
22 high resolution, continental scale, flood mapping, synthetic rating curves (SRCs) were developed
23 across the National Hydrography Dataset (NHDPlusV2) to translate flows, like those generated
24 by the NOAA National Water Model, into river depths. This approach uses Digital Elevation
25 Models (DEM) to define the necessary cross-sectional properties for Manning's equation. A
26 significant limitation, alongside an opportunity for broad improvement, has been assigning
27 suitable roughness without local information. We applied the DEM based methodology to
28 generate SRCs at 7,270 locations with known USGS rating curves, and calibrated roughness to
29 minimize the error between predicted and observed flow. Subsequently, we tested several
30 approaches based on land cover, stream order, and the hydrographic network to estimate the
31 optimized values in a manner that can be extended to ungauged catchments. Among these, a
32 predictive Machine Learning (ML) model based on the NHDPlusV2 network attributes
33 demonstrated superior ability to estimate the optimized roughness with a Spearman correlation
34 of 0.89. Sensitivity analysis showed improving accuracy of DEM and roughness is crucial for
35 accurate estimation of the lower and mid/upper parts of SRC, respectively. Finally, we applied
36 the predictive model over the NHDPlusV2, generating reach-level roughness estimates that can
37 directly support national flood mapping efforts. The method is generalizable to any hydrofabric
38 network that contains topology; however the generated values are dependent on the DEM and
39 hydrofabric used.

40

41 **Plain Language Summary**

42 Synthetic rating curves (SRCs) have been developed for every river segment in the United States
43 as part of the Continental Flood Inundation Mapping Framework (CFIM). A mathematical
44 equation called the Manning's equation and a Digital Elevation Model (DEM) map are the
45 baseline requirements for creating these SRCs. Studies have shown that with careful estimation
46 of roughness, these SRCs can be used to create detailed, real-time flood maps when paired with
47 streamflow simulations like those from the NOAA National Water Model. Normally, channel
48 roughness is estimated from field surveys, model calibration, or tables that ask about the channel
49 and its surroundings. However, in practice, this approach is limited to surveyed locations. Here
50 we used the DEM based SRC methodology to generate SRCs at 7,270 locations with known
51 USGS rating curves. From these we identified the best roughness value that would minimize the
52 error between predicted and observed flow. We tested several approaches for predicting these
53 values including using land cover, stream order, and hydrographic properties of the National
54 Hydrography Dataset (NHDPlusV2). The latter proved most capable at predicting roughness and
55 was applied over the ~2.7 million NHDPlusV2 reaches.

56 **1 Introduction**

57 Stage-discharge relationships are pivotal in flood mapping and routing, providing
58 essential insights into river behavior during flood events (Guerrero et al., 2012; Guven & Aytok,
59 2009). Manning roughness coefficients, which signify channel and floodplain resistance to flow,
60 are integral to refining these relationships (Mansanarez et al., 2019). Accurate estimation of
61 Manning roughness is particularly crucial in ungauged locations, where streamflow data is scarce

62 (Karamouz & Mahani, 2021). By employing empirical relationships, remote sensing data, or land
63 use analysis, hydrologists can estimate Manning roughness coefficients for such areas,
64 improving flood mapping and routing accuracy (Zheng et al., 2018). This enhanced precision
65 aids in better understanding flood dynamics and facilitates more effective flood risk
66 management, ultimately reducing socio-economic impacts associated with floods.

67 Stage-discharge relationships depend on the hydraulic characteristics of the stream
68 channel, are known to vary over time, and are subject to numerous sources of uncertainty,
69 including unstable control, non-uniform flow, and local stage variability (A. Hamilton & Moore,
70 2012; S. Hamilton, 2008; McMahon & Peel, 2019; Muste et al., 2012; Westerberg et al., 2011).
71 A rating curve represents a relationship between two variables, most commonly discharge (Q)
72 and an elevation relative to a datum, more commonly referred to as stage (m). While there are
73 many approaches for establishing rating curves, they broadly include empirical (direct and
74 indirect measurements), mechanical, and theoretical methods. *Direct empirical methods* require
75 streamflow measurements following an approach developed in the 1890s (Kean & Smith, 2005;
76 Rojas et al., 2020). However, obtaining measurements can pose challenges particularly during
77 high flow events and maintenance requires considerable resources leading to an increasing
78 number of defunded gauges (Kean & Smith, 2005). *Indirect empirical methods* employ a variety
79 of flow models that require measured channel geometry, specified water surface elevations, and
80 an empirical roughness value to characterize resistance to flow (Benson & Dalrymple, 1967).
81 Roughness is known to vary with stage and is typically calibrated for a specific set of flow rates
82 (Barnes, 1967; Jarrett, 1984; Kubrak et al., 2019; Limerinos, 1970; Marcus et al., 1992).
83 However, since resistance cannot be assigned without prior knowledge, indirect methods have
84 limited ability to generate complete, stage-discharge relationships (Kean & Smith, 2005).
85 Furthermore, even when calibrated, empirical roughness only captures friction, or skin
86 resistance, while neglecting drag generated by the normal forces acting on a water volume (Kean
87 & Smith, 2005). As a result, *mechanical models* have been used to estimate drag and friction
88 explicitly using in-situ measurements of channel geometry, as well as the physical roughness of
89 the bed, banks, floodplain, and vegetation density (Kean & Smith, 2005). These models have
90 been shown to provide more accurate discharge estimates at a lower cost than many indirect
91 methods (Kean & Smith, 2005, 2010).

92 While observations, empirical, and mechanical methods are ideal, the requirement for on-
93 site measurements limit their application at large scales. Assigning roughness values represents
94 one of the most challenging processes to generalize and is one of the most sensitive parameters
95 in streamflow calculations (Hutton et al., 2012). To provide continental flood forecasts (J
96 Michael Johnson et al., 2019; J. Michael Johnson, Narock, et al., 2022; Maidment, 2016), and
97 enhanced emergency response (Dallo et al., 2020; J Michael Johnson et al., 2018), Zheng et al.
98 (2017) proposed a method to estimate reach-level synthetic ratings curves (SRC) from Digital
99 Elevations Models (DEM) as part of the National Flood Interoperability Experiment (NFIE;
100 Maidment, 2016). This theoretical rating curve method estimates the hydraulic characteristics
101 from a Height Above Nearest Drainage (HAND) raster (Nobre et al., 2011; Rennó et al., 2008)
102 and the National Hydrography Dataset (NHDPlusV2, McKay et al., 2012), making the method
103 extendable to ungauged basins. In the first iteration of the NFIE, and in the following
104 Continental Flood Inundation Mapping framework (CFIM), a default global roughness of 0.05
105 was used. (Zheng et al., 2017) found a global roughness for SRCs resulted in variable accuracy,
106 but also that accurate depth estimates could be achieved for the studied Tar River Watershed by
107 calibrating roughness to a stage-discharge relation produced from HEC-RAS modeling. (Zheng

108 et al., 2018) implemented the HAND approach using a LIDAR DEM, calling the approach
109 ‘GeoFlood’, finding it capable of capturing the Federal Emergency Management Agency
110 (FEMA) flood plain coverage with 60–90% accuracy when adjusting the roughness to best align
111 the SRC to a measured United States Geological Survey (USGS) rating curve. As part of that
112 study, the authors highlighted an extreme sensitivity to even small variations in roughness. Other
113 studies have carried out indirect evaluations of the skill of SRCs by comparing HAND-based
114 inundation maps to remotely sensed flood products and aerial imagery in which the assignment
115 of roughness was identified as a principal limiting factor in accurate flood prediction (Garousi-
116 Nejad et al., 2019; J Michael Johnson et al., 2019). Today, the CFIM approach is actively being
117 developed as an open-source flood inundation mapping software (FIM) operated and maintained
118 by the National Oceanic and Atmospheric Administration’s (NOAA) National Weather Service
119 (NWS) (NOAA-OWP, 2021, p.). In FIM3, a stream order-based roughness is applied to move
120 beyond *default global roughness* values. A study by (Qi & Liu, 2019) demonstrated the
121 importance of considering land-use changes and its significant impact on alteration of roughness
122 coefficient that results in drastic changes in estimated extreme flood peaks.

123 Collectively, this emerging body of evidence recognizes that improved estimates of
124 roughness are crucial for the success of the continental flood mapping framework. The objective
125 of this work is to estimate a national set of reach-level empirical roughness values suitable for
126 theoretical rating curves to enhance operational flood prediction and other hydroscience
127 calculations reliant on estimated roughness. We propose a novel approach for more accurate
128 estimation of roughness using a Machine Learning (ML) model trained on NHDPlusV2 network
129 attributes and compare our results to widely accepted methods for estimating roughness in both
130 academic literature and operational settings. By calculating the explicit spatial representation of
131 roughness within the context of national scale FIM efforts, we directly address many of the
132 shortcomings associated with the static parameterization of roughness, enabling us to more
133 concretely isolate the various sources of error within the SRC. In the *data* section, we outline the
134 datasets used. In the *methods* section, we describe the existing SRC calculation techniques; the
135 methods used to optimize roughness to USGS rating curves, and to estimate roughness based on
136 stream order, land cover, and the hydrofabric network. Lastly, we introduce performance metrics
137 for evaluating model skill. The *discussion* examines SRC performance using the different
138 roughness estimates; how different sections of the rating curves exhibit error; and the sensitivity
139 of SRC generation to the input DEM, hydrofabric, and selected roughness. Finally, the
140 conclusions highlight the implications of this work as well as the limitations of the provided data
141 and opportunities for the continued use of the broader approach.

142 **2 Data**

143 **2.1 Observed USGS Rating Curves**

144 The USGS measures rating curves on a 6–8-weeks schedule and disseminates the
145 information Water Information System (NWIS: <https://waterdata.usgs.gov/nwis/sw>) (Beran &
146 Piasecki, 2008; De Cicco et al., 2018). A sample of 7,270 active USGS rating curves were
147 collected from NWIS, and recorded stage values were converted to depths by subtracting the
148 reported zero-flow stage from all stage values. Normalizing depths to the zero-flow record
149 allows us to estimate the local reference datum by assuming the zero-flow is referenced to the
150 surveyor-defined channel bottom.

151 For each rating curve, a natural cubic spline was fitted and used to estimate stage values
152 for 25 evenly spaced intervals ranging from 0 to the maximum observed streamflow. Observed
153 USGS rating curves are subject to random gage measurement errors and systematic errors
154 resulting from cross section changes, scouring, bed fill and backwater effects (McMillan &
155 Westerberg, 2015). However, we assume these relationships to be accurate at the scale of a
156 continental study, and our goal is to approximate these recorded relationships. Future work can
157 build on extensive studies like those carried out in Australia (McMahon & Peel, 2019) to
158 characterize the uncertainty in the observed ratings.

159 **2.2 Hydrofabric Data**

160 The medium-resolution National Hydrography Dataset Version 2 (NHDPlusV2: 1:100,000 scale)
161 digitally mapped the surface water network of the continental United States (CONUS) into ~2.7
162 million river segments with similar hydrologic characteristics (McKay et al., 2012) NHDPlusV2
163 comprises the original NHD Flowline geometries, the 30-meter National Elevation Dataset, and
164 "value-added attributes" (VAA's) that encompass pre-calculated network characteristics
165 enhancing network analysis. While VAAs are precomputed for NHDPlusV2, they can be
166 generated for any set of hydrofabric data with a topology (D. Blodgett et al., 2020, 2023; D. L.
167 Blodgett & Johnson, 2022a). In this research, we aggregated VAA analysis attributes into single
168 file, accessible as a HydroShare resource (J M Johnson, 2021). Methods for accessing the tabular
169 VAA table were incorporated into the USGS nhdplusTools R package (D. L. Blodgett &
170 Johnson, 2022b) to support this research. By segregating attribute data from geometry, we can
171 more readily use this information in statistical and ML models. In future iterations of hydrofabric
172 whether it be MERIT (Yamazaki et al., 2019), TDX-hydro (McCormack et al., 2022), the
173 USGS/NOAA Reference Fabric (Bock et al., 2022), or the NOAA Next Generation Water
174 Resource Modeling Framework hydrofabric (J. Michael Johnson, 2022), similar characteristics
175 can be computed.

176 **2.3 Height Above Nearest Drainage Data**

177 The Height Above Nearest Drainage (HAND) is a normalized elevation dataset that describes the
178 height of each cell above the nearest designated flow path (Nobre et al., 2011). In 2018, (Y. Y.
179 Liu et al., 2018) generated a HAND dataset for the Continental United States (CONUS) using
180 the 10-meter USGS National Elevation Dataset (NED), the NHDPlusV2, and the D_{∞} distance
181 down calculation available in TauDEM (Tesfa et al., 2011). All HAND data, along with
182 intermediate processing steps, are accessible on the University of Texas (UT) Corral server
183 (<https://web.corral.tacc.utexas.edu/nfiedata/>). This dataset has been updated as part of the
184 Continental Flood Inundation Mapping (CFIM) framework implemented at Oak Ridge National
185 Laboratory (Y. Y. Liu et al., 2020) and was used in this research.

186 **3 Methods**

187 We employed the DEM-based SRC methodology to generate and validate roughness values
188 based on their capacity to replicate streamflow-depth relationships akin to recorded USGS rating
189 curves. In this section, we outline the process of establishing reach level hydraulic properties
190 (3.1), estimating roughness (3.2), comparing SRCs to observed values (3.3), and evaluating the
191 sensitivity of the input parameters (3.4).
192

193 **3.1 Estimation of Reach Average Hydraulic Properties**

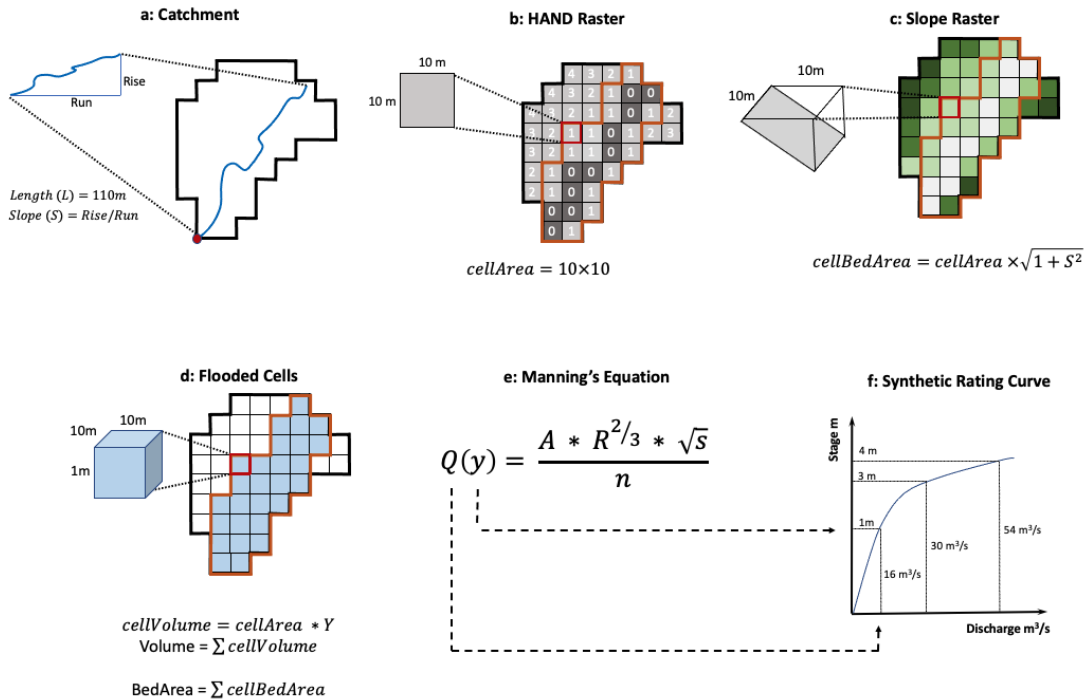
194 Manning’s equation (equation 1) characterizes open channel flow as a function of channel
 195 velocity, flow area, slope, and roughness (Chow, 1959; Farmer et al., 2019; Pavelsky, 2014).
 196 Originally developed for uniform flow conditions where the water-surface profile and energy
 197 gradient are parallel to the streambed, and the cross-sectional area, hydraulic radius, and depth
 198 remain constant throughout the reach. It can be assumed that equation 1 is equally valid for the
 199 nonuniform reaches typically found in floodplains (Jarrett, 1984).

200
 201
$$Q(y) = \frac{A(y) \times R(y)^{2/3} \times \sqrt{S}}{n} \tag{1}$$

202
 203 where:

- 204 $Q(y)$ = the discharge at depth y (m^3/s),
 205 $A(y)$ = the cross-sectional area at depth y (m^2)
 206 $R(y)$ = the hydraulic radius at depth y (m)
 207 S = the longitudinal slope (m/m)
 208 n = the Manning’s roughness coefficient
 209

210 The method proposed by Zheng, Tarborton et al. (2018) calculates cross-sectional area (A),
 211 hydraulic radius (R) and streambed slope (S) from HAND, the hydrofabric information. It
 212 necessitates a user-defined roughness as illustrated in Figure 1. This iterative process is
 213 replicated for a predetermined set of stage (Y) values.
 214



215
 216

217 **Figure 1:** Process for creating stage-discharge relationships as defined in Zheng, Tarboton, et al., (2018).
 218 (a) The catchment boundary establishes contributing cells, and the flowpath length (L) and slope (S) are
 219 then defined by the hydrofabric. (b) The HAND raster stores the elevation above the nearest river cell in
 220 the contributing area. (c) The slope raster defines the effective bed surface area of each cell dependent on
 221 the raster resolution. (d) For a defined stage (e.g., $Y=2$), inundated cells (outlined in orange across panels)
 222 are determined as those where $HAND \leq Y$. The volume and bed area of the inundated cells are then
 223 computed from (b) and (c). (e) Manning's Equation estimates a flow rate Q. (f) A collection of Y-Q
 224 relations defines an SRC.

225 As illustrated in Figure 1a, possible contributing cells (all those that are “nearest a drainage”) are
 226 selected, in this case using the NHDPlusV2 catchment. The NHDPlus VAA attributes provide
 227 the stream length (L; m) and longitudinal slope (S; m/m), and the HAND raster provides the
 228 elevation difference between each grid cell and the nearest flow path. A slope raster (1c) contains
 229 the percent slope (cellSlope) of each grid cell, which can be used to estimate the effective ground
 230 surface or bed area (BA) at a given depth (Equation 2).

$$231 \quad 232 \quad BA = cellres^2 \sqrt{1 + cellslope^2} \quad (2)$$

233 For any defined stage (Y; meters), the HAND raster can be used to identify inundated cells
 234 where the HAND value is less than Y (1d). At each of these cells, a water volume (V) can be
 235 calculated as the depth of ponded water multiplied by the cell area (Equation 3).

$$236 \quad 237 \quad 238 \quad V(y) = cellres^2 \times (Y - HAND) \quad (3)$$

239 For all inundated cells, the total bed area ($\sum BA$) and volume ($\sum V(y)$) can approximate the cross-
 240 sectional area (Equation 4), wetted perimeter (Equation 5), and hydraulic radius (Equation 6)
 241 needed in Manning's Equation (Figure 1e).

242 where:

$$243 \quad 244 \quad 245 \quad 246 \quad A(y) = \sum \frac{V(y)}{L} \quad (4)$$

$$247 \quad 248 \quad WP(y) = \sum \frac{BA(y)}{L} \quad (5)$$

$$249 \quad 250 \quad R(y) = \frac{A(y)}{WP(y)} \quad (6)$$

251 Iterating this calculation over a defined set of depths using a defined single value or stage-
 252 varying roughness yields a streamflow-depth table resembling a rating curve (Figure 1f).

253 **3.2 Estimating the Roughness Terms**

254 In various hydrology subfields, roughness is often estimated based on stream order or
 255 land cover characteristics. Models such as WRF-Hydro assign roughness as a function of
 256 Strahler stream order for overland flow calculation and Muskingum-Cunge hydrograph routing
 257 (Gochis et al., 2016a). In 2016, Li introduced the NHDPlus Inundation Modeler V4.0, which
 258 relies on a separate stream order-based approach (Li, 2016). In both lumped and distributed
 259 hydrologic models, land cover datasets are frequently used to assign roughness through

260 reclassification tables, with similar methodologies applied in dam breach analysis and other 2D
 261 hydrologic and hydraulic models (Janssen, 2016; Kalyanapu et al., 2009; Z. Liu et al., 2019).

262 Furthermore studies have demonstrated that a stage-varying composite roughness (N),
 263 based on defined in-channel and overbank regions may outperform a single roughness value
 264 (Boulomytis et al., 2017; Kubrak et al., 2019; Nguyen & Fenton, 2005). The composite approach
 265 has been shown to reduce error in hydraulic models by as much as 70% for surveyed reaches
 266 (Tuozzolo et al., 2019). Although there are multiple ways to define a composite roughness,
 267 (Tullis, 2012) found Horton's equation (Equation 7: Chow, 1959) to yield the most consistent
 268 results across disparate channel types.

$$270 \quad N = \frac{(P_{ch}(n_1)^{1.5} + P_{ob}(n_2)^{1.5})^{\frac{2}{3}}}{P_{total}^{\frac{2}{3}}} \quad (7)$$

271 Where:

272 N = composite roughness value,

273 n_1 = in-channel n

274 n_2 = overbank n

275 P_{ch} = wetted channel perimeter (m)

276 P_{ob} = wetted overbank perimeter (m)

277 P_{total} = total wetted perimeter (m).

278
 279 In locations where a USGS rating curve is available, we can determine an optimized roughness
 280 by minimizing the error between observed and simulated flows. In locations without a known
 281 rating curve, we can build on prior methodologies and assign single value and composite
 282 roughness values based on stream order or land cover. Additionally, we introduce a ML
 283 approach that leverages the VAAs of the hydrographic network to estimate roughness based on
 284 patterns found in the optimization exercise. Within these approaches, multiple variants are tested,
 285 resulting in eleven unique methods that are described below.

286 **3.2.1 Optimization**

287 Optimized roughness values aim to minimize the error between simulated and observed
 288 discharge for given depths. By fitting the roughness term alone, it is assumed (tested in 3.4) that
 289 uncertainty in other inputs (DEM and hydrofabric) are minimal. To define a single roughness for
 290 each NHDPlusV2 catchment, we solved equation 1 using a nonlinear least squares regression
 291 model (NLS) based on the Gauss-Newton algorithm with 50 maximum iterations, a convergence
 292 tolerance of 1e-09, a lower bound of 0.01, an upper bound of 0.40, and an initial guess of 0.05 (J.
 293 M. Johnson et al., 2024; J. Michael Johnson, Coll, et al., 2022). Considering the DEM and
 294 hydrofabric data as static, the roughness value (n) is the only term in Manning's equation that can
 295 be adjusted via calibration. The lower and upper bounds were selected based on literature-driven
 296 values for reasonable floodplain roughness, with the initial guess derived from the CFIM
 297 precedent. In all cases, the NLS solver converged, and varying the initial guess had no
 298 discernible impact on the estimation in a sample of 500 basins.

299 A composite roughness was defined for each catchment by treating all cells with a
 300 HAND value of 0 as in-channel, and the remaining as out-of-channel. Both n_1 and n_2 were

301 estimated using a NLS model with bounds of (0.01 and 0.20), and (0.01 and 0.40), respectively,
 302 with an initial guess of 0.05 for each. A final constraint ensured that n_i was less than n_{i-1} in each
 303 solution. Multiple starting values were tested in a selected subset of basins with no notable
 304 differences in the results. Combined, the single value and composite optimized results provide a
 305 validation dataset used throughout this research.

306 3.2.2 Stream Order-Based Estimation

307 Previous studies (Cosgrove et al., 2020; Gochis et al., 2016b; Li, 2016) have used stream order
 308 as a proxy for roughness. We aim to evaluate how these approximation tables compare to the
 309 mean and median single value optimized derived from the USGS rating curves. Table 2 presents
 310 these values alongside those used in Li (2016) and the WRF-Hydro/National Water Model
 311 version 2.0 RouteLink file. In the National Water Model implementation of WRF-Hydro, both an
 312 in-channel roughness (n) and a compound channel roughness (n_{CC}) are associated with each
 313 flowline feature of NHDPlus.

314 **Table 1.** Roughness values used for the Stream order approximations
 315

Order	Mean Optimized	Median Optimized	Li-Assignment	WRF-Hydro n	WRF-Hydro n_{CC}
Source			<i>Li (2016)</i>	<i>Gochis (2016)</i>	<i>Gochis (2016)</i>
1	0.196	0.187	0.14	0.060	0.12
2	0.181	0.169	0.12	0.060	0.12
3	0.157	0.134	0.09	0.055	0.11
4	0.128	0.103	0.09	0.055	0.11
5	0.107	0.079	0.07	0.050	0.10
6	0.088	0.057	0.06	0.050	0.10
7	0.083	0.051	0.03	0.045	0.09
8	0.067	0.043	0.03	0.045	0.09
9	0.047	0.029	0.03	0.040	0.08
10	0.043	0.037	0.03	0.040	0.08

316

317 3.2.3 Land Cover Estimation

318 Land cover information can provide a spatially heterogeneous perspective of the
 319 landscape, yet it is prone to sampling and resampling error as well as scale-related classification
 320 uncertainties (J Michael Johnson & Clarke, 2021; Kim et al., 2024). Foster and Maxwell (2019)
 321 identified that vegetation-defined heterogeneity influenced behavior and determined n values in
 322 the stream network, but grid resolution did not reveal a clear scaling relationship. Hence, we are
 323 interested in both single flood plain values, akin to those used in flood mapping studies,
 324 and stage-varying roughness values.

325 The 2019 National Land Cover Database (NLCD) underwent reclassification using
 326 roughness values proposed by Kalyanapu et al. (2009) and extended by Liu et al. (2019). A
 327 single floodplain roughness was calculated for each reach by averaging all cells submerged by
 328 the maximum stage in the rating curve. Furthermore, a stage-varying roughness was generated
 329 by calculating the average land cover roughness using only the inundated cells at each stage.
 330

331 3.2.4 Hydrofabric Gradient Boosted Machines (GBM)

332 Roughness is dependent on a variety of channel characteristics, making it a suitable
 333 candidate for exploration with predictive ML models. After evaluating multiple options, a
 334 Gradient Boosted Machine (GBM) algorithm was selected. GBMs are known to enhance model
 335 generalizability (Friedman, 2001) but due to lack of inherent regularization, and highly complex
 336 decision boundaries they tend to focus on difficult-to-fit data points and result in overfitting.
 337 However, adjusting its hyperparameters and applying early stopping can mitigate this issue. In
 338 contrast to supervised single predictive models or those based on ensemble averages (e.g.,
 339 random forests), GBMs sequentially add new models to an ensemble and update a trained base
 340 learner with each iteration.

341 Fitting GBMs necessitates several hyperparameters, including the number of trees (T); an
 342 interaction depth (K); a learning rate (λ); and subsampling controls (p). The interaction depth
 343 (K) determines the number of splits in each tree and the pace at which the algorithm proceeds
 344 down the gradient descent. Smaller learning rates (λ) reduce the likelihood of overfitting but
 345 prolong the convergence time. While these parameters confer flexibility to GBM models, they
 346 demand intensive tuning to select appropriate values. Hence, a grid of potential hyperparameters
 347 for this problem was defined as follows (Equation 8):
 348
 349

$$350 \text{ hyperparameters} = \left\{ \begin{array}{l} k = 1, 2, \dots, 15 \\ T = 500, 1000, \dots, 5000 \dots 10000, 15000, \dots, 40000 \\ \lambda = 0.001, 0.005, 0.01, \dots, 0.1 \\ R = 5, 10, 15 \\ p = 0.3 \end{array} \right\} \quad (8)$$

351 To identify the variables that most accurately predict roughness, we defined a training dataset
 352 using a stratified random sampling method, selecting 500 or 80% of the gauged locations from
 353 each HUC2 from the Watershed Boundary Dataset. Developing a GBM approach involves a
 354 three-step process.

355 *Step 1:*

356 Initially, a series of 16,065 GBMs were fitted for each hyperparameter combination (Equation 8),
 357 using all numeric variables from the NHDPlusV2 VAA as predictors. For each model,
 358 the relative influence of each predictor was computed in addition to the number of times it was
 359 selected for splitting, weighted by the squared improvement provided at each split. These results
 360 were averaged over all trees (Friedman, 2001), and those with the highest relative influence were
 361 paired with a subjective evaluation of how easily they could be computed for general hydrofabric
 362 networks, yielding the final set of 5 core predictors:
 363

- 364 i. **Drainage Area:** Drainage area (km²) of the single flowpath catchment
- 365 ii. **Flowpath Length:** Flowline length in kilometers
- 366 iii. **Arbolate Sum:** The cumulative length of the upstream drainage network (mainstem and
 367 tributaries) from the outlet of the catchment
- 368 iv. **Path Length:** The distance from the flowline outlet to the end of the network along the
 369 mainstem path
- 370 v. **Slope:** A unitless fraction (cm/cm) of the flow path slope derived from the 30m NED

371 **Step 2:**

372 Using only these five predictors, a new set of 16,065 GBMs was trained for all hyperparameter
 373 combinations, and the combination producing the minimal RMSE was selected to train a final
 374 model. That model used the following:

- 375
 376 i. $k = 12$
 377 ii. $T = 40,000$
 378 iii. $\lambda = 0.025$
 379 iv. $R = 10$
 380 v. $p = 0.3$

381 Upon completion, the predicted roughness values generated with this model had an RMSE of
 382 0.045, and a nRMSE of 26.4%, when compared to the single value optimized roughness values.

383 **Step 3:**

384 Using the model trained in step 2, we predicted roughness across the NHDPlusV2 network.
 385 Similarly, any river segment with a known drainage area, flowpath length, arbolate sum, path
 386 length, and slope can serve as input to develop a predicted single value roughness. It is critical to
 387 note that the predicted values are unique to the input NHDPlusV2 dataset; extrapolation or
 388 conflation to a different network would likely provide poor results. Nonetheless, new data can
 389 be generated from the model provided a network topology is known

390 **3.3 Synthetic Rating Curve Comparison**

391 This optimized roughness (n), a standard default value (0.05), a stream order based, land cover
 392 based, and GBM approaches produce eleven synthetic (and one observed) rating curve at each of
 393 the 7, 270 gauged locations. For clarity, these methods are summarized in Table 2.

394
 395 **Table 2:** Methods and approaches for assigning roughness for rating curves

#	Category	Name	Description
1	observed	USGS	25 evenly distributed Q-Y points built from a cubic spline fit to the observed USGS rating curve
2	default	global-roughness	Roughness of 0.05 assigned to all reaches
3	optimized	single-value	Single roughness, fit to the observed rating curve using a non-linear solver with a lower and upper bound of 0.01 and 0.4.
4	optimized	composite	Composite roughness using Horton's method where n_1 and n_2 were fit to the observed rating curve using a non-linear solver with a lower and upper bound of {0.01, 0.01} and {0.2, 0.4}.
5	stream order	Li-assignment	Roughness assigned by stream order based on Li, 2016
6	stream order	wrf-N	Roughness assigned by stream order from the 'Manning's roughness' (n) in the NWM v2.1 RouteLink file
7	stream order	wrf-Ncc	Roughness assigned by stream order from the 'Compound Channel Manning's n ' (nCC) in the NWM v2.0 RouteLink file
8	stream order	mean-optimized	Roughness assigned by stream order based on mean values from the calibrated method
9	stream order	median-optimized	Roughness assigned by stream order based on median values from the calibrated method

10	land cover	single-value	Single value assigned via a reclassified land cover map using those values submerged by maximum RC stage
11	land cover	stage-varying	Stage varying values assigned via a reclassified land cover map using cells submerged by the current RC stage
12	hydrofabric	GBM	Values assigned based on output of trained GBM model using the NHDPlus VAA attributes as predictor variables

396
397
398
399
400

To assess SRC accuracy, the simulated discharge values produced with each roughness, using the USGS rating curve stage values, were compared to the USGS discharge values using the root mean squared error normalized to the mean of observed discharge (nRMSE; see Equation 9).

$$nRMSE = 100 \times \sqrt{\frac{(Q_{src} - Q_{obs})^2}{Q_{obs}}} \quad (9)$$

401
402
403
404
405
406

where:

$$Q_{obs} = \text{observed discharge}$$

$$Q_{src} = \text{simulated discharge.}$$

407
408
409
410
411
412

nRMSE was calculated for the entire rating curve as well as the lower, middle, and upper sections. While defining “good” and “bad” nRMSE is subjective, a cut off of 30% nRMSE has been used to determine whether a site displays reasonable performance in prior research (Gleason & Smith, 2014; Yoon et al., 2016). For readability throughout the text, we adopt this shorthand and describe errors of 30% or less as reasonable, and errors of 100% or more as extreme.

413

3.4 Parameter Sensitivity

414
415
416
417

One open question about SRCs is how sensitive the results are to input data including the DEM, hydrofabric, and roughness. To decompose the SRC into its primary components, Manning’s Equation can be rewritten by substituting equations 4, 5, 6 into equation 1, and rearranging such that:

418
419

$$Q(y) = V \times \frac{1}{n} \times \frac{1}{L} \times \sqrt{S} \quad (10)$$

420
421

Where

422

$$V = \frac{Vol(y)^{\frac{5}{3}}}{BA(y)^{\frac{2}{3}}}$$

423
424
425
426
427
428
429
430
431

To understand the role of each of the input dataset in streamflow estimation, we want to perform sensitivity analyses with respect to the four uncertain parameters - V, n, L, and S - by implementing a separate sensitivity analysis at stages 1, 2, 3 ... 25 using a factorial design.

To build the factorial design for sensitivity analysis, we need to establish reasonable range bands for each of these variables that are adjustable to each site. The volume factors are driven by the DEM which is most easily influenced by the vertical accuracy as highlighted in case studies leveraging LIDAR (Zheng et al., 2018). The 10m NED has a documented vertical accuracy of 3.04 meters (Gesch et al., 2014) so we elected a test set of 0.5, 1 and 2 meters in the

432 positive and negative directions basin wide. These were implemented by adjusting the HAND
433 values throughout a given catchment prior to estimating volume and bed area.

434 To test roughness, we allow roughness to range from 0%, 10%, 25%, 50%, 100% and
435 200% error from the optimized single-value estimates while enforcing the lower and upper limits
436 of 0.01 and 0.40. Length is a byproduct of the hydrofabric resolution and higher resolution data
437 inputs like the NHD High-Resolution will likely increase reach length as more detail is captured.
438 Following research aligning multi-scalar flowline data from the EPA River Reach, Medium
439 Resolution NHDPlus and High Resolution NHD through the identification of common
440 mainstems (D. Blodgett et al., 2020), a high-level comparison revealed a range of variability
441 which we reduced to 0%, 5%, 10% and 15% percent of the NHDPlusV2 flowline values in the
442 positive and negative direction.

443 Slope is a product of the hydrofabric and underlying DEM. While the HAND and Slope
444 rasters are based on the 10m NED, the NHDPlus flowline slope is an attribute derived from the
445 30m NED. A random sample of 100 flowlines from this study were used to extract transects
446 from the 10m NED. The difference between the smoothed slopes of these transects (5 point
447 rolling mean) and the listed slope attributes of the NHDPlus were represented as a 0%, 25%,
448 50% and 75% error in each direction of the recorded values.

449 Using these possible variations, 363 randomly sampled sites were evaluated to ensure
450 accuracy at the 95% confidence level. The results of the design were analyzed with an Analysis
451 of Variance (ANOVA) method to deduce the main effects and two factor interactions using the
452 *multisensi* R package (Bidot et al., 2018). Upon completion, the results were averaged across
453 locations.

454 **4 Results**

455 A total of 81,070 synthetic rating curves (SRCs) were computed for comparison. Section
456 4.1 describes the performance of each roughness method, section 4.2 addresses errors exhibited
457 in each section of the rating curve, section 4.3 addresses the skill of the GBM model, and section
458 4.4 looks at the sensitivity of the SRCs to the roughness, DEM, and hydrofabric inputs used in
459 Manning's equation.

460 **4.1 Synthetic Rating Curve Performance Analysis**

461 Figure 2A illustrates the percentage of locations achieving reasonable and extreme error
462 for each roughness method, alongside the Spearman Correlation compared to the optimized
463 single value roughness. In the outlined section of the table, the 25th, 50th, and 75th quartile (Q1,
464 Q2, Q3) nRMSE for the complete rating curve, and the mean nRMSE for each section of the
465 rating curve are displayed. These statistics are derived solely from sites producing nRMSE <
466 100% for that method.

467 The two optimized approaches provide the least error across all metrics but are confined
468 to gaged locations. SRCs generated with an optimized composite roughness offer marginal
469 improvement over those with an optimized single value, and occasionally exhibit degraded
470 performance. This implies that a composite view, particularly when considering locations where
471 HAND = 0 as in channel, is not critical to SRC roughness estimation. The optimized single value
472 approach achieved reasonable error in ~80% of the tested locations, suggesting models
473 potential accuracy across a broad spectrum of locations. Nonetheless, the remaining 20%
474 highlight areas where the HAND-based SRC model may be incomplete or other sources of
475 uncertainty contribute to the error.

476 Amongst methods extendable to ungaged basins, the GBM method demonstrates superior
477 results and notably reduced error compared to stream order and land cover approaches. Notably,
478 it generates nearly four times as many SRCs with reasonable error as other nonsite optimized
479 methods. The correlation with the optimized single value is also double compared to the next
480 closest method.

481 All four stream order methods exhibit similar performance metrics and offer marginal
482 improvement over the global default. Stream order information primarily reduces the number of
483 sites with extreme error ($nRMSE > 100\%$). This is done best by the mean optimized stream order
484 values. This performance improvement over a global default value emphasizes that roughness is
485 a local phenomenon, and the thematic assignment is too generalized to provide significant
486 performance gains. The two land cover methods demonstrate identical performance, with neither
487 land cover method offering an improvement over the stream order methods, and added
488 substantial computational burden.

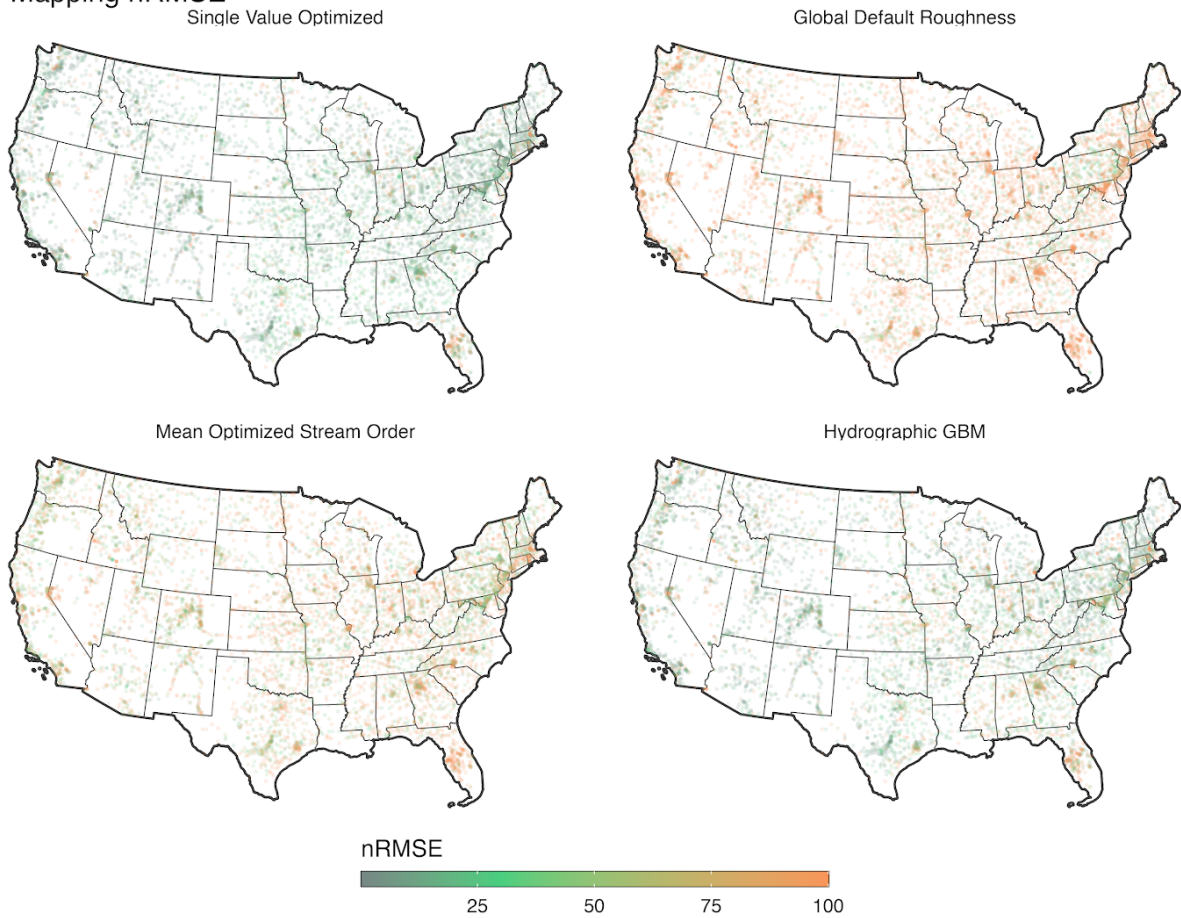
489 Finally, a default global roughness of 0.05 achieves $nRMSE \leq 30\%$ in just 10% of the
490 locations emphasizing the need for a spatially heterogeneous approach and the value in seeking a
491 more sophisticated approach. To visualize these statistical patterns spatially, Figure 2B maps the
492 $nRMSE$ from the best performing method for each approach. While the magnitudes of error in
493 the optimized and GBM methods differ, the maps highlight regions of the country where large
494 errors persist across all methods. Prominent examples include the gulf coast of Florida, the
495 eastern seaboard, the Atlanta metro region, and to a lesser extent, the lower Mississippi
496 floodplain.

497

A. Evaluation Metrics

Method	Approach	nRMSE	nRMSE	Correlation with Optimized	Q1	Q2	Q3	mean nRMSE	mean nRMSE	mean nRMSE
		≤30%	>100%		nRMSE	nRMSE	nRMSE	lower	middle	upper
Single Value	Optimized	78.10	8.81	1.00	6.14	11.88	21.58	40.22	15.79	11.73
Composite N	Optimized	76.74	10.32	NA	4.62	10.54	20.86	37.12	15.16	11.20
GBM	Hydrographic	61.85	16.21	0.88	7.46	14.76	31.38	44.70	22.40	18.61
Median Optimized	Stream Order	16.10	40.37	0.44	28.53	49.13	71.63	58.11	44.18	42.39
Mean Optimized	Stream Order	15.74	35.21	0.43	30.65	52.60	74.27	60.15	46.35	44.33
Li Assignment	Stream Order	15.09	46.29	0.41	27.74	48.10	72.06	57.90	43.83	42.08
wrf-nCC	Stream Order	14.59	40.51	0.40	30.42	51.80	73.52	59.93	46.03	43.88
wrf-n	Stream Order	12.15	59.52	0.40	25.95	46.53	73.16	56.60	43.06	42.09
Single Value	Land cover	11.50	34.74	-0.05	38.00	63.57	82.95	64.98	52.66	51.15
Stage-Varying	Land cover	11.32	34.66	NA	38.01	63.53	82.74	64.52	52.42	51.20
Global roughness	Default	11.28	61.32	NA	26.60	48.09	73.87	57.20	43.52	42.56

B. Mapping nRMSE



498
499

500 **Figure 2:** (a) Synthetic rating curve accuracy across methods. Quartile error values and the percentage of
501 sites with reasonable and extreme errors are listed. The methods are sorted by the Q2 criteria, and darker
502 hues represent better performance and are applied column-wise. (b) The nRMSE from each method is
503 mapped.

504 Across all methods, there is consistently more error in the lower section of the rating
505 curve compared to the middle and upper portions. SRCs developed with a global default and
506 mean optimized stream order have the highest mean nRMSE across all sections of the curve. The

507 single value optimized and hydrofabric GBM approaches both reduce the mean nRMSE in each
 508 section; however, the error remains higher by a factor of 2+ in the lower third. This pattern may
 509 have to do with (1) lack of bathymetric representation in HAND data for in-channel flows, (2)
 510 the datum adjustment applied to achieve a zero-flow USGS rating curve, or (3) that at smaller
 511 flows/depths, small errors are more impactful than the errors at higher flows/depths.
 512 Nonetheless, estimated SRCs demonstrate greater accuracy at the higher end of the rating curve,
 513 which holds promise for flood mapping studies and other use cases. Moreover, this staggered
 514 performance suggests the potential to optimize n for various sections of the rating curve based on
 515 flow which could be provided by the National Water Model. While a composite n was not found
 516 to be a valuable addition, a stage-varying n might offer improvements.

517 **4.2 Model and Optimized Skill**

518 The error for the single-value optimized method provides the best possible result given
 519 the current DEM, hydrofabric, and roughness bounded to the range of $\{0.01, 0.4\}$. Taking the
 520 DEM and hydrofabric data as static, the only term in Manning's equation that can be calibrated is
 521 the roughness value. The roughness value serves as a proxy for representing the ratio of water
 522 volume to discharge. Very large n values represent situations where a very strong resistance to
 523 flow is used to reduce discharge when HAND volumes are large for a given stage, but the actual
 524 SRC derived discharge is low. Very low values of n represent the opposite situation where
 525 calculated water volumes based on HAND properties are low but the required discharge is quite
 526 large. This observation may suggest a need to represent channel bathymetry to accommodate
 527 excess HAND water volumes. This section focuses on comparisons between the single optimized
 528 value and GBM approaches, particularly the cases where the imposed lower and upper limits
 529 were reached – likely to address issues in other inputs to Manning's equation.

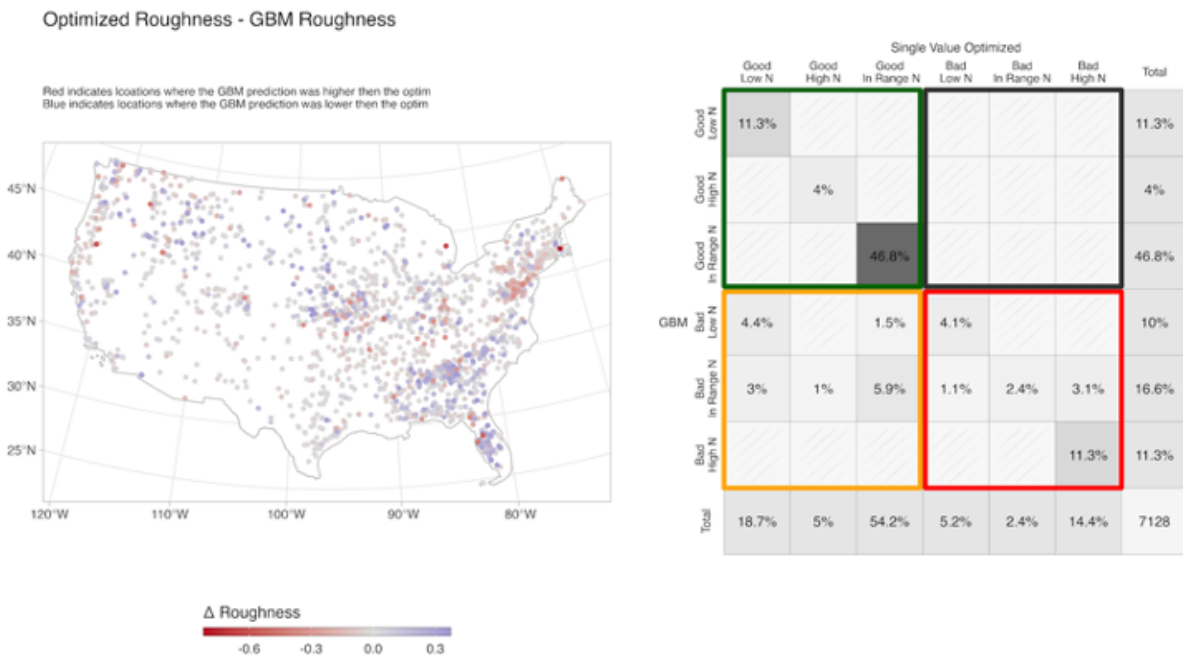
530 The error for the single-value optimized method provides the best possible result given
 531 the current DEM, hydrofabric, and roughness bounded to the range of $\{0.01, 0.4\}$. Figure 3A
 532 shows the difference in roughness between the optimized and GBM approach. Sites with an
 533 absolute value of $\Delta N < 0.01$ have been removed from the map. In this Figure, sites that appear
 534 red indicate that the N value of the GBM based on network attributes is greater than the
 535 optimized n value; conversely, sites that are blue indicate the opposite. On the East coast, we
 536 observe a landscape where the GBM tends to show greater roughness compared to the optimized
 537 values while in the southeast, the GBM tends to show lower N . The rest of the country indicates
 538 a more mixed approach, with a slight tendency for the GBM to predict n lower than the
 539 optimized approach (blue).

540 Next, we categorized the *skill* of the rating curve (by the nRMSE $< 30\%$ threshold) and
 541 whether the roughness pushed toward the upper limit (>0.35), the lower limit (<0.05), or was
 542 within a fair range ($0.05 \leq n \leq 0.35$). In total, this yielded six categories that were used to classify
 543 the GBM and optimized-based SRCs. Figure 3B shows the confusion matrix of these divided
 544 into four color-coded quadrants while Figure 3C shows categorical classification. The first
 545 column (green and orange box) represents the total number of sites that were well-served by the
 546 site-by-site optimization. In total, 77.9% of the locations achieved reasonable error, and 54.2%
 547 did so without stretching the roughness value toward the imposed limits. For those that did push
 548 roughness towards an imposed limit, the bulk stretched towards the low value. This highlights
 549 the tendency of the GBM model to favor lower roughness and a broader notion that HAND
 550 volumes tend to under-predict the actual volume flowing through the river channel. The first row
 551 (green and black box) represents the total number of sites that were well-served by the GBM

552 model. In total, 62.1% of the sites were able to achieve reasonable error, with ~15% stretching
553 the roughness value toward the imposed limits.

554 Starting in the upper left, the green section shows that 62.1% of sites achieve a
555 reasonable nRMSE in both the single-value optimization and GBM. 46.8% of these did so with
556 an in-range roughness, while ~15% pushed the upper and lower limits. Specifically, there is a
557 strong preference to push the optimization roughness towards the lower limit of 0.01. Moving
558 counterclockwise, the black box is empty, highlighting that the GBM cannot find solutions
559 where the optimization failed. The red box represents situations where both the optimization and
560 GBM methods were unable to find a solution. The implicit concern is that the errors in the input
561 data are larger than what roughness adjustments alone can correct in ~22% of the tested
562 locations.

563 In total, 17.8% of sites produced bad optimizations with the same pattern for both site-
564 based optimized and GBM methods. For example if a site had a bad nRMSE with a low n, the
565 GBM produced the same which is encouraging for the skill of the GBM, but suggests future
566 work might look to eliminate these sites in the model training. In the remaining 4.2% percent, the
567 GBM took on a low or high optimized n, and brought it into the expected range without
568 improving the performance.



Percent of sites per stream order that fall into each classification

Single Site Optimized Approach

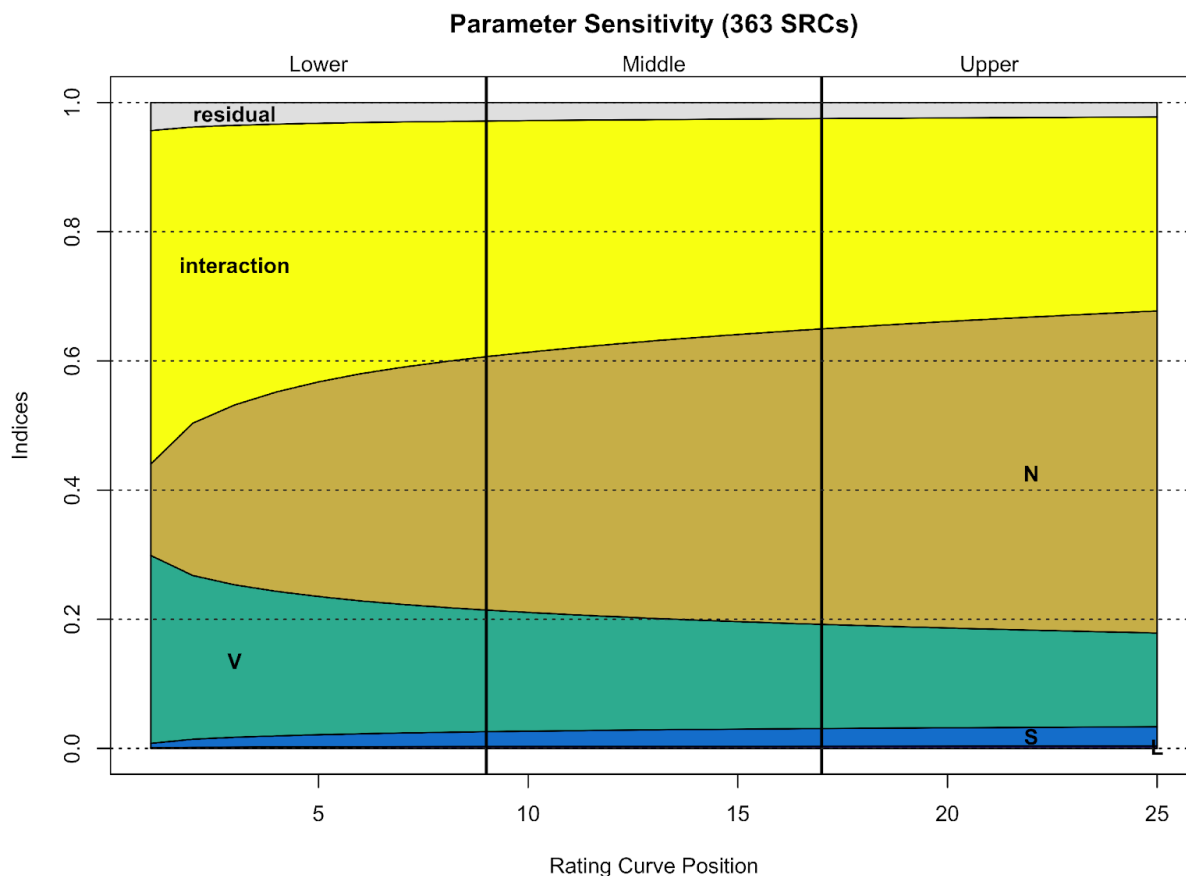
	Order 1	Order 2	Order 3	Order 4	Order 5	Order 6	Order 7	Order 8	Order 9	Order 10
Good High N	6.8	8.8	8.6	5.4	3.4	2.6	3.0	0.0	0	0
Bad High N	56.8	33.3	17.2	9.7	6.5	4.8	5.7	6.0	4	0
Good Low N	2.4	3.9	8.6	16.2	25.8	35.6	38.3	40.5	40	50
Bad Low N	0.5	1.3	1.3	3.4	7.6	10.6	10.5	21.4	24	0
Good In Range N	31.2	50.5	61.1	62.6	54.2	44.2	39.2	31.0	28	50
Bad In Range N	2.4	2.2	3.2	2.7	2.5	2.1	3.3	1.2	4	0

569
570
571 **Figure 3:** (a) The difference in roughness produced by the GBM and Optimized roughness values are
572 mapped. Red (negative values) indicate locations where the GBM prediction produces higher values than
573 the optimized approach. Blue (positive values) indicate locations where the GBM prediction produces
574 roughness lower than the optimized approach. Sites where the difference was less than ± 0.01 were
575 excluded (b) The GBM and single site optimized results were categorized by the skill of the rating curve
576 (by the nRMSE < 30% threshold), and whether the roughness pushed toward the upper limit (>0.35), the
577 lower limit (<0.05), or was within the range ($0.05 \leq N \leq 0.35$). (c) The percent of sites, per stream order,
578 that fall into each classification. Darker hues represent larger percentages. The horizontal line after order
579 4 represented a break in SRC creation performance identified in prior research.

580 **4.3 Parameter Sensitivity**

581 In this section we investigate the sensitivity of SRCs to the primary inputs using factorial
582 design and ANOVA decomposition, which include the (1) DEM, (2) hydrofabric, and (3)

583 roughness. Figure 4 shows the sensitivity indices of the main effects and first-order interactions
 584 at each point in the rating curve normalized to 1.



585
 586 **Figure 4:** Evolution of the main effects and the first-order interaction sensitivity indices of the SRC
 587 variables averaged over 363 randomly selected locations.

588 In the lower third of the rating curve, there is more sensitivity to the DEM (V), interaction terms,
 589 and residual effects. This suggests that SRCs perform worse in the lower third of the rating curve
 590 largely because they are more easily influenced by multiple factors. Starting around the middle
 591 of the rating curve, proportional sensitivity starts to stabilize with ~15% being contributed by the
 592 DEM, ~45% by roughness, and ~30% from variable interaction. There is minimal error (in total
 593 ~10%) contributed from the length, slope, or residual effects of the model combined. It is notable
 594 that as one approaches the upper end of the curve, the contribution of error from the interaction
 595 and V terms decrease further and are generally overtaken by sensitivity to roughness.

596 These results indicate that the primary challenge in developing accurate SRCs is
 597 Manning's roughness for mid and high SRC values, and very low SRCs are affected by DEM
 598 errors and missing bathymetry, but there are other key sources of uncertainty. The overwhelming
 599 sensitivity to roughness means that areas suffering from other inputs can only be identified when
 600 the uncertainty in roughness is minimized. Given that the primary objective of many operational
 601 flood inundation forecasting systems is to warn of high magnitude events, optimization of
 602 roughness for this objective seems practical. For those seeking predictive skill for lower

603 magnitude events, i.e., “nuisance” flooding, improving accuracy of base information such as the
604 DEM seems to be more critical.

605 Aside from roughness and the interaction of all inputs, the volume of water computed
606 from the DEM was the largest source of error. As the USGS 3D elevation program moves their
607 elevation program towards the collection of nationally comprehensive and complete LIDAR
608 coverage, it is worth mentioning here the possible opportunities and limitations with the method
609 provided here.

610 **5 Discussion**

611 A challenging aspect of the transferability of our proposed methodology is the scale-
612 dependency of both DEM that plays a crucial role in generating water volume for a given depth
613 defined by a HAND product, and hydrographic properties that are used for roughness
614 calculations. Ideally we would like the trained roughness ML model to be transferable to any
615 other hydrographic network generated at different scales. We conjecture that this holds true for
616 networks of comparable scale (i.e., 1:100,000 ratio). Another question is whether the assumption
617 that the variable selected during the feature importance analysis remains consistent as
618 hydrographic network scale changes? For instance in higher resolution networks, characterized
619 by the prevalence of more tributaries with greater sinuosity, the arbolate sum, a key
620 characteristic, typically demonstrates a notable increase. Consequently, if a smaller river system
621 within the higher resolution network is trained solely on lower resolution data, it might
622 erroneously exhibit attributes akin to those of a much larger system, potentially resulting in
623 artificially low roughness values.

624 Similar to hydrographic scale impact on roughness, the higher resolution LiDAR or DEM
625 data improves accuracy in channel volume estimation and synthetic rating curve calculation by
626 providing detailed terrain data, enhancing channel morphology representation, and minimizing
627 uncertainties in channel geometry and hydraulic modeling. This contributes to more reliable
628 assessments of water resources and flood risks. The utilization of LiDAR data holds promise for
629 mitigating uncertainty in volume estimations through several mechanisms. The first method, akin
630 to that employed in GeoFlood, involves increasing the horizontal (grid) resolution to yield more
631 effective “cells.” This reduction in resampling inherently enhances the vertical accuracy at each
632 cell. The second method entails utilizing LiDAR to refine vertical accuracy within the same 10m
633 grid as the current 3DEP 10m product, effectively integrating the latest data captures to enhance
634 the existing grid. In both scenarios, if a new DEM is utilized, recalibration of the base inputs to a
635 Synthetic Rating Curve (SRC) – namely, the cross-sectional area and hydraulic radius at depth Y
636 – following the methodology outlined by Zheng et al. (2017) is necessary. This entails updating
637 the GBM model based on the full hyperparameter set (Step 2) but does not necessitate retraining
638 on the complete set of VAA attributes (Step 1).

639 Despite the potential enhancements to the current DEM, the issue of changing scales (cell
640 resolution) raises an open question. To qualitatively assess the transferability of GBM-produced
641 roughness values across DEM scales, we compared the reported, tuned roughness values at five
642 USGS sites examined in Zheng et al. (2018) to the GBM values. While the GBM approach
643 tended to overpredict roughness compared to the reported GeoFlood values, a correlation was
644 observed (albeit from a limited dataset). This trend aligns with the notion that larger grid cells
645 yield larger volumes and, per equation 11, necessitate larger roughness values. The idea that
646 roughness varies with DEM resolution finds support in hydrologic modeling research. For
647 example, it has been established that 2D flood models are sensitive to DEM resolution (Fewtrell

648 et al., 2008; Horritt & Bates, 2002; Saksena & Merwade, 2015; Schumann et al., 2007), and
649 roughness (Lim et al., 2016; Mason et al., 2003; Pappenberger et al., 2005). However, conflicting
650 findings exist regarding the existence of a scaling relationship, with some studies suggesting
651 otherwise (M. Foster & M. Maxwell, 2019). Hence, it is acknowledged that the dependency of
652 GBM roughness values on DEM and hydrography constitutes a limitation of the dataset
653 produced herein, not the methodology. Future investigations will explore methods for
654 operationalizing roughness model fitting and prediction based on the methods and data (USGS
655 rating curves) developed in this study.

656 An assessment of the sites exhibiting extreme error in SRC with the calibrated n values
657 demonstrated that SRC extreme error often occurs when roughness approaches one of the
658 enforced physical limits. It was also in these areas where the largest divergence between the
659 predicted and calibrated n values was observed. In many ways, this divergence in n values offers
660 a signal for when other aspects of the SRC creation are uncharacteristically influential. The value
661 of n serves as a proxy for representing the ratio of water volume to discharge. Very large n
662 values represent situations where a very strong resistance to flow is used to reduce discharge
663 when HAND volumes are large for a given stage, but the actual SRC derived discharge is low.
664 Very low values of n represent the opposite situation where calculated water volumes based on
665 HAND properties are low but the required discharge is quite large. (perhaps suggesting a need
666 for representing channel bathymetry to accommodate excess HAND water volumes).

667 Finally, several critical considerations arise when utilizing this dataset or extending the
668 workflow beyond its current scope. The workflow, beginning with a mechanical measurement of
669 roughness to train a predictive model based on network attributes, subsequently utilized the same
670 network and DEM to establish a relationship between water surface height and discharge
671 required for that stage. However, the applicability of these findings to variations in input
672 parameters, such as alterations to the underlying network, remains unclear. Further inquiry is
673 warranted to determine whether the values derived from this dataset could be used as a direct
674 crosswalk to the new network, whether the values would need to be recalculated based on the
675 new attributes of the network using the existing model, whether the model would need retraining
676 using the new inputs, or whether the process of determining the selected features needs to be
677 performed.

678 **6 Conclusions**

679 At the onset of this research, the necessity for improved reach-level roughness was
680 highlighted to support continental flood mapping efforts. We employed the methodology
681 proposed by Zheng et al. (2017) to define reach-averaged hydraulic traits from a 10m HAND
682 product in catchments with a USGS gauge and calibrated a roughness value to minimize the
683 error in predicted flows. This approach resulted in 78% of gaged locations achieving $nRMSE \leq$
684 30%. To produce SRCs in ungauged basins, we evaluated a range of methods for estimating
685 reach-level roughness. Among these, a data-driven ML model based on NHDPlus hydrographic
686 topology proved the most robust. The ML model produced almost four times the number of
687 SRCs with acceptable error compared to non-optimizable methods (e.g., stream order and land
688 cover methods). Additionally, its correlation with the optimized single value is twice that of the
689 next closest method. The predictions were able to achieve a ranked correlation of 0.89 with the
690 optimized values and SRCs with reasonable error in 62% of the tested locations. In contrast, a
691 widely used global roughness value captured just 13% of SRCs with reasonable error, and the
692 best performing stream order parameterization captured just 16%.

693 A sensitivity test showed that the DEM and roughness are the principal sources of error
694 in the conceptual rating curve model, while length and slope are practically non-significant. We
695 demonstrated that as the upper end of the SRC is approached, it becomes apparent that the
696 contribution of error from the interaction and V terms decrease further and are generally
697 overtaken by sensitivity of roughness. These conclusions are generally in line with other work
698 that has looked at HAND-based SRC uncertainty at individual sites (Godbout et al., 2019). The
699 conclusion is that in locations where roughness is the primary contributor of uncertainty, the data
700 driven roughness and existing data inputs can produce reasonable SRCs. In areas where the
701 DEM and hydrography introduce uncertainty, the calibrated values take on a role that was not
702 *per se* roughness, but rather a broad error-reducing scalar. Such locations were not pervasive,
703 and generally clustered around regions with large built-up extents, known engineered controls, or
704 low relief. In these areas where DEM fidelity is a primary source of SRC error, there is capacity
705 for LIDAR to be used with the methods suggested as part of the GeoFlood project (Zheng et al.,
706 2018). A drawback to using LIDAR is the availability, procurement costs, and computational
707 needs associated with creating HAND and generating inundation forecasts at large scales.
708 Fortunately, the 10m DEM seems serviceable for the majority of CONUS, and the SRC error
709 map (Figure 2) can help prioritize areas where the integration of LIDAR data might be especially
710 beneficial.

711 Future work will involve exploring several avenues to address key findings in this
712 research and potential implications. Firstly, we demonstrated a disparity in error across different
713 sections of the rating curve, particularly higher error in the lower section compared to the middle
714 and upper portions. This signals a need to evaluate the absence of bathymetry in the model, as
715 the missing channel volume likely impacts the lower end of the rating curve. Secondly, the
716 findings suggest promising prospects for FIM methods that rely on Synthetic Rating Curves
717 (SRCs) for high flow applications. Thirdly, there is potential for optimizing the roughness
718 coefficient (n) for various sections of the rating curve. While a composite n was not found to be
719 beneficial, a stage-varying n might prove advantageous. Lastly, future research will explore how
720 this method scales across different networks, assessing its applicability and performance in
721 diverse hydrological settings. Within the United States, LIDAR may provide better discretization
722 and some additional bathymetry data. The effects of this can be tested at reaches that have both
723 LIDAR and USGS rating curves. These datasets can be effective in training a ML model and
724 gaining a better understanding of the effect of grid cells and data driven roughness on model
725 training. In essence, further research may be able to quantify how more location-attuned
726 roughness values can contribute to improved large-scale hydrologic routing and other
727 applications of reach-level roughness.

728 For regions outside the USA, official stream network data similar to the NHD are few
729 and far between. Publicly available data are often aggregated at lower spatial resolutions,
730 decreasing the ability to represent the full drainage network. However, the rapid increase in the
731 amount of crowd-sourced stream network data available through platforms like OpenStreetMap
732 offers the promise of high-resolution data that can be used for improved global reach level
733 modeling for smaller rivers. Localized high-resolution official drainage networks, crowd-sourced
734 stream network data offer the opportunity to evaluate the impact of scale, network density, and
735 attributes on the ability of GBM models to characterize the rating curve relationship. Overall, the
736 value of the current work lies in the data produced for the scale of the medium-resolution NHD
737 and 10m 3DEP product, as well as a method and curated set of training data to apply to other
738 scales within and outside the United States. The roughness values have been made publicly

739 available on HydroShare with easy-access options for both R and Python. With respect to R, the
 740 roughness values can be accessed with the nhdplusTools *get_vaa* functionalities. We hope the
 741 use of this data can support improved flood forecasting, applications that need to estimate
 742 roughness, and can prompt consideration of what other hydrologic properties and characteristics
 743 can be learned and supported by the topology implicit to hydrography datasets.

744

745 **Acknowledgments**

746 Parts of writing this work were performed with funding from the National Science Foundation's
 747 Urban Flooding Open Knowledge Network Center (Grants 1937099, 2033607). Any opinions,
 748 findings, and conclusions or recommendations expressed in this material are those of the authors
 749 and do not reflect the views of the National Science Foundation.

750

751 **Disclaimer**

752 The views expressed in this article do not necessarily represent the views of NOAA or the United
 753 States.

754

755 **Open Research**

756 The roughness values generated in the research are available at (J M Johnson, 2021). The GBM
 757 model is available at <https://github.com/LynkerIntel/hydrofabricML>. A version of this software
 758 will be published through Zenodo after the review process to accommodate for any needed
 759 changes.

760

761 **References**

- 762 Barnes, H. H. (1967). *Roughness characteristics of natural channels*. US Government Printing Office.
 763 Benson, M. A., & Dalrymple, T. (1967). *General field and office procedures for indirect discharge measurements*.
 764 US Govt. Print. Off.,.
 765 Beran, B., & Piasecki, M. (2008). Availability and coverage of hydrologic data in the US geological survey National
 766 Water Information System (NWIS) and US Environmental Protection Agency Storage and Retrieval
 767 System (STORET). *Earth Science Informatics*, 1(3–4), 119–129.
 768 Bidot, C., Lamboni, M., & Monod, H. (2018). Multisensi: Multivariate sensitivity analysis. *R Package Version*, 2,
 769 1–1.
 770 Blodgett, D., Johnson, J. M., Sondheim, M., Wieczorek, M., & Frazier, N. (2020). Mainstems: A logical data model
 771 implementing mainstem and drainage basin feature types based on WaterML2 Part 3: HY_Features
 772 concepts. *Environmental Modelling & Software*, 104927.
 773 Blodgett, D., Johnson, J. M., & Bock, A. (2023). Generating a reference flow network with improved connectivity to
 774 support durable data integration and reproducibility in the coterminous US. *Environmental Modelling &*
 775 *Software*, 165, 105726.
 776 Blodgett, D. L., & Johnson, J. M. (2022a). Hydrologic modeling and river corridor applications of HY_Features
 777 concepts. Retrieved from <http://www.opengis.net/doc/PER/22-040>
 778 Blodgett, D. L., & Johnson, J. M. (2022b). nhdplusTools: Tools for Accessing and Working with the NHDPlus.
 779 Bock, A., Blodgett, D. L., Johnson, J. M., Santiago, M., & Wieczorek, M.E. (2022). *National Hydrologic Geospatial*
 780 *Fabric Reference and Derived Hydrofabrics: U.S. Geological Survey data release*. Retrieved from
 781 <https://doi.org/10.5066/P9NFPB5S>
 782 Boulomytis, V. T. G., Zuffo, A. C., Dalfré Filho, J. G., & Imteaz, M. A. (2017). Estimation and calibration of
 783 Manning's roughness coefficients for ungaged watersheds on coastal floodplains. *International Journal of*
 784 *River Basin Management*, 15(2), 199–206.
 785 Chow, V. T. (1959). Open-channel hydraulics. *McGraw-Hill Civil Engineering Series*.
 786 Cosgrove, B. A., Gochis, D. J., Clark, E. P., & Flowers, T. (2020, January 13). NOAA's National Water Model: A
 787 Dynamically Evolving Operational Hydrologic Forecasting Framework. American Meteorological Society.
 788 Retrieved from <https://ams.confex.com/ams/2020Annual/webprogram/Paper365698.html>

- 789 Dallo, I., Stauffacher, M., & Marti, M. (2020). What defines the success of maps and additional information on a
790 multi-hazard platform? *International Journal of Disaster Risk Reduction*, 49, 101761.
- 791 De Cicco, L. A., Lorenz, D., Hirsch, R. M., Watkins, W., & Johnson, M. (2018). *dataRetrieval: R packages for*
792 *discovering and retrieving water data available from U.S. federal hydrologic web services* (manual).
793 Reston, VA: U.S. Geological Survey / U.S. Geological Survey. <https://doi.org/10.5066/P9X4L3GE>
- 794 Farmer, W. H., LaFontaine, J. H., & Hay, L. E. (2019). Calibration of the US geological survey national hydrologic
795 model in ungauged basins using statistical at-site streamflow simulations. *Journal of Hydrologic*
796 *Engineering*, 24(11), 04019049.
- 797 Fewtrell, T., Bates, P. D., Horritt, M., & Hunter, N. (2008). Evaluating the effect of scale in flood inundation
798 modelling in urban environments. *Hydrological Processes: An International Journal*, 22(26), 5107–5118.
- 799 Friedman, J. H. (2001). Greedy function approximation: a gradient boosting machine. *Annals of Statistics*, 1189–
800 1232.
- 801 Garousi-Nejad, I., Tarboton, D. G., Aboutaleb, M., & Torres-Rua, A. F. (2019). Terrain Analysis Enhancements to
802 the Height Above Nearest Drainage Flood Inundation Mapping Method. *Water Resources Research*,
803 55(10), 7983–8009. <https://doi.org/10.1029/2019WR024837>
- 804 Gesch, D. B., Oimoen, M. J., & Evans, G. A. (2014). *Accuracy assessment of the US Geological Survey National*
805 *Elevation Dataset, and comparison with other large-area elevation datasets: SRTM and ASTER* (No.
806 2331–1258). US Geological Survey.
- 807 Gleason, C. J., & Smith, L. C. (2014). Toward global mapping of river discharge using satellite images and at-many-
808 stations hydraulic geometry. *Proceedings of the National Academy of Sciences*, 111(13), 4788–4791.
- 809 Gochis, D., Dugger, A., McCreight, J., Karsten, L. R., Logan, Yu, W., et al. (2016a). *Technical Description of the*
810 *National Water Model Implementation of WRF-Hydro*.
- 811 Gochis, D., Dugger, A., McCreight, J., Karsten, L. R., Logan, Yu, W., et al. (2016b). *Technical Description of the*
812 *National Water Model Implementation of WRF-Hydro*.
- 813 Godbout, L., Zheng, J. Y., Dey, S., Eyclade, D., Maidment, D., & Passalacqua, P. (2019). Error assessment for
814 height above the nearest drainage inundation mapping. *JAWRA Journal of the American Water Resources*
815 *Association*, 55(4), 952–963.
- 816 Guerrero, J.-L., Westerberg, I. K., Halldin, S., Xu, C.-Y., & Lundin, L.-C. (2012). Temporal variability in stage–
817 discharge relationships. *Journal of Hydrology*, 446, 90–102.
- 818 Guven, A., & Aytok, A. (2009). New Approach for Stage–Discharge Relationship: Gene-Expression Programming.
819 *Journal of Hydrologic Engineering*, 14(8), 812–820. [https://doi.org/10.1061/\(ASCE\)HE.1943-5584.0000044](https://doi.org/10.1061/(ASCE)HE.1943-5584.0000044)
- 820 Hamilton, A., & Moore, R. (2012). Quantifying Uncertainty in Streamflow Records. *Canadian Water Resources*
821 *Journal/Revue Canadienne Des Ressources Hydriques*, 37(1), 3–21.
- 822 Hamilton, S. (2008). Sources of uncertainty in Canadian low flow hydrometric data. *Canadian Water Resources*
823 *Journal*, 33(2), 125–136.
- 824 Horritt, M., & Bates, P. (2002). Evaluation of 1D and 2D numerical models for predicting river flood inundation.
825 *Journal of Hydrology*, 268(1–4), 87–99.
- 826 Hutton, C. J., Brazier, R. E., Nicholas, A. P., & Nearing, M. (2012). On the effects of improved cross-section
827 representation in one-dimensional flow routing models applied to ephemeral rivers. *Water Resources*
828 *Research*, 48(4), 2011WR011298. <https://doi.org/10.1029/2011WR011298>
- 829 Janssen, C. (2016). Manning’s n Values for Various Land Covers To Use for Dam Breach Analyses by NRCS in
830 Kansas. PAC.
- 831 Jarrett, R. D. (1984). Hydraulics of high-gradient streams. *Journal of Hydraulic Engineering*, 110(11), 1519–1539.
- 832 Johnson, J M. (2021). NHDPlus Value Added Attributes - no geometries. HydroShare. Retrieved from
833 <https://www.hydroshare.org/resource/6092c8a62fac45be97a09bfd0b0bf726/>
- 834 Johnson, J. M., Afshari, S., & Rad, A. M. (2024). AHGestimation: An R package for computing robust, mass
835 preserving hydraulic geometries and rating curves. *JOSS (in Review)*.
- 836 Johnson, J. Michael. (2022). National Hydrologic Geospatial Fabric (hydrofabric) for the Next Generation
837 (NextGen) Hydrologic Modeling Framework. HydroShare. Retrieved from
838 <http://www.hydroshare.org/resource/129787b468aa4d55ace7b124ed27dbde>
- 839 Johnson, J Michael, & Clarke, K. C. (2021). An area preserving method for improved categorical raster resampling.
840 *Cartography and Geographic Information Science*, 1–13.
- 841 Johnson, J Michael, Coll, J. M., Ruess, P. J., & Hastings, J. T. (2018). Challenges and Opportunities for Creating
842 Intelligent Hazard Alerts: The “FloodHippo” Prototype. *Journal of the American Water Resources*
843 *Association*.
- 844

- 845 Johnson, J Michael, Munasinghe, D., Eyelade, D., & Cohen, S. (2019). An Integrated Evaluation of the National
846 Water Model (NWM)–Height Above Nearest Drainage (HAND) Flood Mapping Methodology. *Natural*
847 *Hazards and Earth System Sciences*, 19(11), 2405–2420.
- 848 Johnson, J. Michael, Coll, J., Clarke, K. C., Afshari, S., Saksena, S., & Yeghiazarian, L. (2022). Determining
849 Feature Based Hydraulic Geometry and Rating Curves using a Physically Based, Computationally Efficient
850 Framework. Retrieved from <https://www.preprints.org/manuscript/202212.0390>
- 851 Johnson, J. Michael, Narock, T., Singh-Mohudpur, J., Fils, D., Clarke, K. C., Saksena, S., et al. (2022). Knowledge
852 graphs to support real-time flood impact evaluation. *AI Magazine*, 43(1), 40–45.
853 <https://doi.org/10.1002/aaai.12035>
- 854 Kalyanapu, A. J., Burian, S. J., & McPherson, T. N. (2009). Effect of land use-based surface roughness on
855 hydrologic model output. *Journal of Spatial Hydrology*, 9(2).
- 856 Karamouz, M., & Mahani, F. F. (2021). DEM Uncertainty Based Coastal Flood Inundation Modeling Considering
857 Water Quality Impacts. *Water Resources Management*, 35(10), 3083–3103.
858 <https://doi.org/10.1007/s11269-021-02849-9>
- 859 Kean, J. W., & Smith, J. D. (2005). Generation and verification of theoretical rating curves in the Whitewater River
860 basin, Kansas. *Journal of Geophysical Research: Earth Surface*, 110(F4).
- 861 Kean, J. W., & Smith, J. D. (2010). Calculation of stage-discharge relations for gravel bedded channels. *Journal of*
862 *Geophysical Research: Earth Surface*, 115(F3).
- 863 Kim, D.-H., Johnson, J. M., Clarke, K. C., & McMillan, H. K. (2024). Untangling the impacts of land cover
864 representation and resampling in distributed hydrological model predictions. *Environmental Modelling &*
865 *Software*, 172, 105893.
- 866 Kubrak, E., Kubrak, J., Koziol, A., Kiczko, A., & Krukowski, M. (2019). Apparent Friction Coefficient Used for
867 Flow Calculation in Straight Compound Channels. *Water*, 11(4), 745.
- 868 Li, Z. (2016, June). *A Framework of ArcGIS-Based Flood Inundation Modeling and Mapping System*,. Presented at
869 the ESRI Proceedings, ESRI Proceedings. Retrieved from
870 https://proceedings.esri.com/library/userconf/proc16/papers/265_671.pdf
- 871 Lim, N. J., Brandt, S. A., & Seipel, S. (2016). Visualisation and evaluation of flood uncertainties based on ensemble
872 modelling. *International Journal of Geographical Information Science*, 30(2), 240–262.
- 873 Limerinos, J. T. (1970). Determination of the Manning coefficient from measured bed roughness in natural
874 channels.
- 875 Liu, Y. Y., Maidment, D. R., Tarboton, D. G., Zheng, X., & Wang, S. (2018). A CyberGIS Integration and
876 Computation Framework for High-Resolution Continental-Scale Flood Inundation Mapping. *Journal of the*
877 *American Water Resources Association*.
- 878 Liu, Y. Y., Tarboton, D. G., & Maidment, D. R. (2020, June 1). Height Above Nearest Drainage (HAND) and
879 Hydraulic Property Table for CONUS - Version 0.2.1. (20200601). (Version Version 0.2.1). Oak Ridge
880 Leadership Computing Facility. Retrieved from 10.13139/ORNLNCCS/1630903
- 881 Liu, Z., Merwade, V., & Jafarzaghan, K. (2019). Investigating the role of model structure and surface roughness in
882 generating flood inundation extents using one-and two-dimensional hydraulic models. *Journal of Flood*
883 *Risk Management*, 12(1), e12347.
- 884 M. Foster, L., & M. Maxwell, R. (2019). Sensitivity analysis of hydraulic conductivity and Manning's n parameters
885 lead to new method to scale effective hydraulic conductivity across model resolutions. *Hydrological*
886 *Processes*, 33(3), 332–349.
- 887 Maidment, D. R. (2016). Conceptual Framework for the National Flood Interoperability Experiment. *JAWRA*
888 *Journal of the American Water Resources Association*, 53(2), 245–257.
- 889 Mansanarez, V., Renard, B., Coz, J. L., Lang, M., & Darienzo, M. (2019). Shift Happens! Adjusting Stage-
890 Discharge Rating Curves to Morphological Changes at Known Times. *Water Resources Research*, 55(4),
891 2876–2899. <https://doi.org/10.1029/2018WR023389>
- 892 Marcus, W. A., Roberts, K., Harvey, L., & Tackman, G. (1992). An evaluation of methods for estimating Manning's
893 n in small mountain streams. *Mountain Research and Development*, 227–239.
- 894 Mason, D. C., Cobby, D. M., Horritt, M. S., & Bates, P. D. (2003). Floodplain friction parameterization in two-
895 dimensional river flood models using vegetation heights derived from airborne scanning laser altimetry.
896 *Hydrological Processes*, 17(9), 1711–1732.
- 897 McCormack, K. A., Levin, H. K., Morris, A. L., Fredericks, J. G., Huening, V., Tavakoly, A., et al. (2022).
898 Validation of TDX-Hydro; a global, TanDEM-X derived, 12m resolution hydrographic data suite. In *AGU*
899 *Fall Meeting Abstracts* (Vol. 2022, pp. H43B-06). Retrieved from
900 <https://ui.adsabs.harvard.edu/abs/2022AGUFM.H43B..06M/abstract>

- 901 McKay, L., Bondelid, T., Dewald, T., Johnston, J., Moore, R., & Rea, A. (2012). NHDPlus Version 2: user guide.
902 *US Environmental Protection Agency*.
- 903 McMahon, T. A., & Peel, M. C. (2019). Uncertainty in stage–discharge rating curves: application to Australian
904 Hydrologic Reference Stations data. *Hydrological Sciences Journal*, 64(3), 255–275.
- 905 McMillan, H., & Westerberg, I. (2015). Rating curve estimation under epistemic uncertainty. *Hydrological
906 Processes*, 29(7), 1873–1882.
- 907 Muste, M., Lee, K., & Bertrand-Krajewski, J.-L. (2012). Standardized uncertainty analysis for hydrometry: a review
908 of relevant approaches and implementation examples. *Hydrological Sciences Journal*, 57(4), 643–667.
- 909 Nguyen, H., & Fenton, J. (2005). Identification of roughness in compound channels (pp. 2512–2518). Presented at
910 the MODSIM 2005 international congress on modelling and simulation. Modelling and Simulation Society
911 of Australia and New Zealand.
- 912 Nobre, A. D., Cuartas, L. A., Hodnett, M., Rennó, C. D., Rodrigues, G., Silveira, A., et al. (2011). Height Above the
913 Nearest Drainage—a hydrologically relevant new terrain model. *Journal of Hydrology*, 404(1–2), 13–29.
- 914 Pappenberger, F., Beven, K., Horritt, M., & Blazkova, S. (2005). Uncertainty in the calibration of effective
915 roughness parameters in HEC-RAS using inundation and downstream level observations. *Journal of
916 Hydrology*, 302(1–4), 46–69.
- 917 Pavelsky, T. M. (2014). Using width-based rating curves from spatially discontinuous satellite imagery to monitor
918 river discharge. *Hydrological Processes*, 28(6), 3035–3040.
- 919 Qi, W., & Liu, J. (2019). Studies on changes in extreme flood peaks resulting from land-use changes need to
920 consider roughness variations. *Hydrological Sciences Journal*, 64(16), 2015–2024.
921 <https://doi.org/10.1080/02626667.2019.1669039>
- 922 Rennó, C. D., Nobre, A. D., Cuartas, L. A., Soares, J. V., Hodnett, M. G., Tomasella, J., & Waterloo, M. J. (2008).
923 HAND, a new terrain descriptor using SRTM-DEM: Mapping terra-firme rainforest environments in
924 Amazonia. *Remote Sensing of Environment*, 112(9), 3469–3481.
- 925 Rojas, M., Quintero, F., & Krajewski, W. F. (2020). Performance of the national water model in iowa using
926 independent observations. *JAWRA Journal of the American Water Resources Association*, 56(4), 568–585.
- 927 Saksena, S., & Merwade, V. (2015). Incorporating the effect of DEM resolution and accuracy for improved flood
928 inundation mapping. *Journal of Hydrology*, 530, 180–194.
- 929 Schumann, G., Matgen, P., Hoffmann, L., Hostache, R., Pappenberger, F., & Pfister, L. (2007). Deriving distributed
930 roughness values from satellite radar data for flood inundation modelling. *Journal of Hydrology*, 344(1–2),
931 96–111.
- 932 Tesfa, T. K., Tarboton, D. G., Watson, D. W., Schreuders, K. A., Baker, M. E., & Wallace, R. M. (2011). Extraction
933 of Hydrological Proximity Measures from DEMs Using Parallel Processing. *Environmental Modelling &
934 Software*, 26(12), 1696–1709.
- 935 Tullis, B. P. (2012). *Hydraulic loss coefficients for culverts* (Vol. 734). Transportation Research Board.
- 936 Tuozzolo, S., Langhorst, T., de Moraes Frasson, R. P., Pavelsky, T., Durand, M., & Schobelock, J. J. (2019). The
937 impact of reach averaging Manning’s equation for an in-situ dataset of water surface elevation, width, and
938 slope. *Journal of Hydrology*, 578, 123866.
- 939 Westerberg, I., Guerrero, J., Seibert, J., Beven, K., & Halldin, S. (2011). Stage-discharge uncertainty derived with a
940 non-stationary rating curve in the Choluteca River, Honduras. *Hydrological Processes*, 25(4), 603–613.
- 941 Yamazaki, D., Ikeshima, D., Sosa, J., Bates, P. D., Allen, G. H., & Pavelsky, T. M. (2019). MERIT Hydro: A High-
942 Resolution Global Hydrography Map Based on Latest Topography Dataset. *Water Resources Research*,
943 55(6), 5053–5073. <https://doi.org/10.1029/2019WR024873>
- 944 Yoon, Y., Beighley, E., Lee, H., Pavelsky, T., & Allen, G. (2016). Estimating flood discharges in reservoir-regulated
945 river basins by integrating synthetic SWOT satellite observations and hydrologic modeling. *Journal of
946 Hydrologic Engineering*, 21(4), 05015030.
- 947 Zheng, X., Tarboton, D. G., Maidment, D. R., Liu, Y. Y., & Passalacqua, P. (2017). River channel geometry and
948 rating curve estimation using height above the nearest drainage. *Journal of the American Water Resources
949 Association*.
- 950 Zheng, X., Maidment, D. R., Tarboton, D. G., Liu, Y. Y., & Passalacqua, P. (2018). GeoFlood: Large-Scale Flood
951 Inundation Mapping Based on High-Resolution Terrain Analysis. *Water Resources Research*.
- 952

19 **Abstract**

20 Rating curves are commonly developed through direct observation, open channel flow models,
21 or mechanical methods, each relying on in-situ measurement. As part of a U.S. effort to provide
22 high resolution, continental scale, flood mapping, synthetic rating curves (SRCs) were developed
23 across the National Hydrography Dataset (NHDPlusV2) to translate flows, like those generated
24 by the NOAA National Water Model, into river depths. This approach uses Digital Elevation
25 Models (DEM) to define the necessary cross-sectional properties for Manning's equation. A
26 significant limitation, alongside an opportunity for broad improvement, has been assigning
27 suitable roughness without local information. We applied the DEM based methodology to
28 generate SRCs at 7,270 locations with known USGS rating curves, and calibrated roughness to
29 minimize the error between predicted and observed flow. Subsequently, we tested several
30 approaches based on land cover, stream order, and the hydrographic network to estimate the
31 optimized values in a manner that can be extended to ungauged catchments. Among these, a
32 predictive Machine Learning (ML) model based on the NHDPlusV2 network attributes
33 demonstrated superior ability to estimate the optimized roughness with a Spearman correlation
34 of 0.89. Sensitivity analysis showed improving accuracy of DEM and roughness is crucial for
35 accurate estimation of the lower and mid/upper parts of SRC, respectively. Finally, we applied
36 the predictive model over the NHDPlusV2, generating reach-level roughness estimates that can
37 directly support national flood mapping efforts. The method is generalizable to any hydrofabric
38 network that contains topology; however the generated values are dependent on the DEM and
39 hydrofabric used.

40

41 **Plain Language Summary**

42 Synthetic rating curves (SRCs) have been developed for every river segment in the United States
43 as part of the Continental Flood Inundation Mapping Framework (CFIM). A mathematical
44 equation called the Manning's equation and a Digital Elevation Model (DEM) map are the
45 baseline requirements for creating these SRCs. Studies have shown that with careful estimation
46 of roughness, these SRCs can be used to create detailed, real-time flood maps when paired with
47 streamflow simulations like those from the NOAA National Water Model. Normally, channel
48 roughness is estimated from field surveys, model calibration, or tables that ask about the channel
49 and its surroundings. However, in practice, this approach is limited to surveyed locations. Here
50 we used the DEM based SRC methodology to generate SRCs at 7,270 locations with known
51 USGS rating curves. From these we identified the best roughness value that would minimize the
52 error between predicted and observed flow. We tested several approaches for predicting these
53 values including using land cover, stream order, and hydrographic properties of the National
54 Hydrography Dataset (NHDPlusV2). The latter proved most capable at predicting roughness and
55 was applied over the ~2.7 million NHDPlusV2 reaches.

56 **1 Introduction**

57 Stage-discharge relationships are pivotal in flood mapping and routing, providing
58 essential insights into river behavior during flood events (Guerrero et al., 2012; Guven & Aytek,
59 2009). Manning roughness coefficients, which signify channel and floodplain resistance to flow,
60 are integral to refining these relationships (Mansanarez et al., 2019). Accurate estimation of
61 Manning roughness is particularly crucial in ungauged locations, where streamflow data is scarce

62 (Karamouz & Mahani, 2021). By employing empirical relationships, remote sensing data, or land
63 use analysis, hydrologists can estimate Manning roughness coefficients for such areas,
64 improving flood mapping and routing accuracy (Zheng et al., 2018). This enhanced precision
65 aids in better understanding flood dynamics and facilitates more effective flood risk
66 management, ultimately reducing socio-economic impacts associated with floods.

67 Stage-discharge relationships depend on the hydraulic characteristics of the stream
68 channel, are known to vary over time, and are subject to numerous sources of uncertainty,
69 including unstable control, non-uniform flow, and local stage variability (A. Hamilton & Moore,
70 2012; S. Hamilton, 2008; McMahon & Peel, 2019; Muste et al., 2012; Westerberg et al., 2011).
71 A rating curve represents a relationship between two variables, most commonly discharge (Q)
72 and an elevation relative to a datum, more commonly referred to as stage (m). While there are
73 many approaches for establishing rating curves, they broadly include empirical (direct and
74 indirect measurements), mechanical, and theoretical methods. *Direct empirical methods* require
75 streamflow measurements following an approach developed in the 1890s (Kean & Smith, 2005;
76 Rojas et al., 2020). However, obtaining measurements can pose challenges particularly during
77 high flow events and maintenance requires considerable resources leading to an increasing
78 number of defunded gauges (Kean & Smith, 2005). *Indirect empirical methods* employ a variety
79 of flow models that require measured channel geometry, specified water surface elevations, and
80 an empirical roughness value to characterize resistance to flow (Benson & Dalrymple, 1967).
81 Roughness is known to vary with stage and is typically calibrated for a specific set of flow rates
82 (Barnes, 1967; Jarrett, 1984; Kubrak et al., 2019; Limerinos, 1970; Marcus et al., 1992).
83 However, since resistance cannot be assigned without prior knowledge, indirect methods have
84 limited ability to generate complete, stage-discharge relationships (Kean & Smith, 2005).
85 Furthermore, even when calibrated, empirical roughness only captures friction, or skin
86 resistance, while neglecting drag generated by the normal forces acting on a water volume (Kean
87 & Smith, 2005). As a result, *mechanical models* have been used to estimate drag and friction
88 explicitly using in-situ measurements of channel geometry, as well as the physical roughness of
89 the bed, banks, floodplain, and vegetation density (Kean & Smith, 2005). These models have
90 been shown to provide more accurate discharge estimates at a lower cost than many indirect
91 methods (Kean & Smith, 2005, 2010).

92 While observations, empirical, and mechanical methods are ideal, the requirement for on-
93 site measurements limit their application at large scales. Assigning roughness values represents
94 one of the most challenging processes to generalize and is one of the most sensitive parameters
95 in streamflow calculations (Hutton et al., 2012). To provide continental flood forecasts (J
96 Michael Johnson et al., 2019; J. Michael Johnson, Narock, et al., 2022; Maidment, 2016), and
97 enhanced emergency response (Dallo et al., 2020; J Michael Johnson et al., 2018), Zheng et al.
98 (2017) proposed a method to estimate reach-level synthetic ratings curves (SRC) from Digital
99 Elevations Models (DEM) as part of the National Flood Interoperability Experiment (NFIE;
100 Maidment, 2016). This theoretical rating curve method estimates the hydraulic characteristics
101 from a Height Above Nearest Drainage (HAND) raster (Nobre et al., 2011; Rennó et al., 2008)
102 and the National Hydrography Dataset (NHDPlusV2, McKay et al., 2012), making the method
103 extendable to ungauged basins. In the first iteration of the NFIE, and in the following
104 Continental Flood Inundation Mapping framework (CFIM), a default global roughness of 0.05
105 was used. (Zheng et al., 2017) found a global roughness for SRCs resulted in variable accuracy,
106 but also that accurate depth estimates could be achieved for the studied Tar River Watershed by
107 calibrating roughness to a stage-discharge relation produced from HEC-RAS modeling. (Zheng

108 et al., 2018) implemented the HAND approach using a LIDAR DEM, calling the approach
109 ‘GeoFlood’, finding it capable of capturing the Federal Emergency Management Agency
110 (FEMA) flood plain coverage with 60–90% accuracy when adjusting the roughness to best align
111 the SRC to a measured United States Geological Survey (USGS) rating curve. As part of that
112 study, the authors highlighted an extreme sensitivity to even small variations in roughness. Other
113 studies have carried out indirect evaluations of the skill of SRCs by comparing HAND-based
114 inundation maps to remotely sensed flood products and aerial imagery in which the assignment
115 of roughness was identified as a principal limiting factor in accurate flood prediction (Garousi-
116 Nejad et al., 2019; J Michael Johnson et al., 2019). Today, the CFIM approach is actively being
117 developed as an open-source flood inundation mapping software (FIM) operated and maintained
118 by the National Oceanic and Atmospheric Administration’s (NOAA) National Weather Service
119 (NWS) (NOAA-OWP, 2021, p.). In FIM3, a stream order-based roughness is applied to move
120 beyond *default global roughness* values. A study by (Qi & Liu, 2019) demonstrated the
121 importance of considering land-use changes and its significant impact on alteration of roughness
122 coefficient that results in drastic changes in estimated extreme flood peaks.

123 Collectively, this emerging body of evidence recognizes that improved estimates of
124 roughness are crucial for the success of the continental flood mapping framework. The objective
125 of this work is to estimate a national set of reach-level empirical roughness values suitable for
126 theoretical rating curves to enhance operational flood prediction and other hydroscience
127 calculations reliant on estimated roughness. We propose a novel approach for more accurate
128 estimation of roughness using a Machine Learning (ML) model trained on NHDPlusV2 network
129 attributes and compare our results to widely accepted methods for estimating roughness in both
130 academic literature and operational settings. By calculating the explicit spatial representation of
131 roughness within the context of national scale FIM efforts, we directly address many of the
132 shortcomings associated with the static parameterization of roughness, enabling us to more
133 concretely isolate the various sources of error within the SRC. In the *data* section, we outline the
134 datasets used. In the *methods* section, we describe the existing SRC calculation techniques; the
135 methods used to optimize roughness to USGS rating curves, and to estimate roughness based on
136 stream order, land cover, and the hydrofabric network. Lastly, we introduce performance metrics
137 for evaluating model skill. The *discussion* examines SRC performance using the different
138 roughness estimates; how different sections of the rating curves exhibit error; and the sensitivity
139 of SRC generation to the input DEM, hydrofabric, and selected roughness. Finally, the
140 conclusions highlight the implications of this work as well as the limitations of the provided data
141 and opportunities for the continued use of the broader approach.

142 **2 Data**

143 **2.1 Observed USGS Rating Curves**

144 The USGS measures rating curves on a 6–8-weeks schedule and disseminates the
145 information Water Information System (NWIS: <https://waterdata.usgs.gov/nwis/sw>) (Beran &
146 Piasecki, 2008; De Cicco et al., 2018). A sample of 7,270 active USGS rating curves were
147 collected from NWIS, and recorded stage values were converted to depths by subtracting the
148 reported zero-flow stage from all stage values. Normalizing depths to the zero-flow record
149 allows us to estimate the local reference datum by assuming the zero-flow is referenced to the
150 surveyor-defined channel bottom.

151 For each rating curve, a natural cubic spline was fitted and used to estimate stage values
152 for 25 evenly spaced intervals ranging from 0 to the maximum observed streamflow. Observed
153 USGS rating curves are subject to random gage measurement errors and systematic errors
154 resulting from cross section changes, scouring, bed fill and backwater effects (McMillan &
155 Westerberg, 2015). However, we assume these relationships to be accurate at the scale of a
156 continental study, and our goal is to approximate these recorded relationships. Future work can
157 build on extensive studies like those carried out in Australia (McMahon & Peel, 2019) to
158 characterize the uncertainty in the observed ratings.

159 **2.2 Hydrofabric Data**

160 The medium-resolution National Hydrography Dataset Version 2 (NHDPlusV2: 1:100,000 scale)
161 digitally mapped the surface water network of the continental United States (CONUS) into ~2.7
162 million river segments with similar hydrologic characteristics (McKay et al., 2012) NHDPlusV2
163 comprises the original NHD Flowline geometries, the 30-meter National Elevation Dataset, and
164 "value-added attributes" (VAA's) that encompass pre-calculated network characteristics
165 enhancing network analysis. While VAAs are precomputed for NHDPlusV2, they can be
166 generated for any set of hydrofabric data with a topology (D. Blodgett et al., 2020, 2023; D. L.
167 Blodgett & Johnson, 2022a). In this research, we aggregated VAA analysis attributes into single
168 file, accessible as a HydroShare resource (J M Johnson, 2021). Methods for accessing the tabular
169 VAA table were incorporated into the USGS nhdplusTools R package (D. L. Blodgett &
170 Johnson, 2022b) to support this research. By segregating attribute data from geometry, we can
171 more readily use this information in statistical and ML models. In future iterations of hydrofabric
172 whether it be MERIT (Yamazaki et al., 2019), TDX-hydro (McCormack et al., 2022), the
173 USGS/NOAA Reference Fabric (Bock et al., 2022), or the NOAA Next Generation Water
174 Resource Modeling Framework hydrofabric (J. Michael Johnson, 2022), similar characteristics
175 can be computed.

176 **2.3 Height Above Nearest Drainage Data**

177 The Height Above Nearest Drainage (HAND) is a normalized elevation dataset that describes the
178 height of each cell above the nearest designated flow path (Nobre et al., 2011). In 2018, (Y. Y.
179 Liu et al., 2018) generated a HAND dataset for the Continental United States (CONUS) using
180 the 10-meter USGS National Elevation Dataset (NED), the NHDPlusV2, and the D_{∞} distance
181 down calculation available in TauDEM (Tesfa et al., 2011). All HAND data, along with
182 intermediate processing steps, are accessible on the University of Texas (UT) Corral server
183 (<https://web.corral.tacc.utexas.edu/nfiedata/>). This dataset has been updated as part of the
184 Continental Flood Inundation Mapping (CFIM) framework implemented at Oak Ridge National
185 Laboratory (Y. Y. Liu et al., 2020) and was used in this research.

186 **3 Methods**

187 We employed the DEM-based SRC methodology to generate and validate roughness values
188 based on their capacity to replicate streamflow-depth relationships akin to recorded USGS rating
189 curves. In this section, we outline the process of establishing reach level hydraulic properties
190 (3.1), estimating roughness (3.2), comparing SRCs to observed values (3.3), and evaluating the
191 sensitivity of the input parameters (3.4).

192

193 **3.1 Estimation of Reach Average Hydraulic Properties**

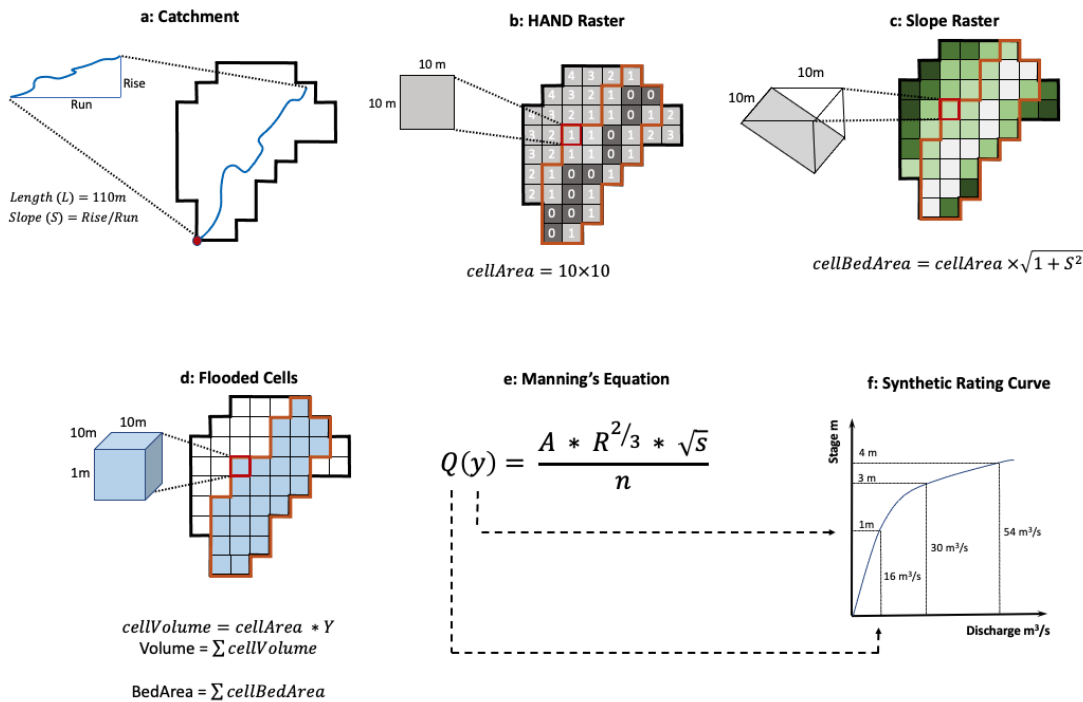
194 Manning’s equation (equation 1) characterizes open channel flow as a function of channel
 195 velocity, flow area, slope, and roughness (Chow, 1959; Farmer et al., 2019; Pavelsky, 2014).
 196 Originally developed for uniform flow conditions where the water-surface profile and energy
 197 gradient are parallel to the streambed, and the cross-sectional area, hydraulic radius, and depth
 198 remain constant throughout the reach. It can be assumed that equation 1 is equally valid for the
 199 nonuniform reaches typically found in floodplains (Jarrett, 1984).

200
 201
$$Q(y) = \frac{A(y) \times R(y)^{2/3} \times \sqrt{S}}{n} \tag{1}$$

202
 203 where:

- 204 $Q(y)$ = the discharge at depth y (m^3/s),
 205 $A(y)$ = the cross-sectional area at depth y (m^2)
 206 $R(y)$ = the hydraulic radius at depth y (m)
 207 S = the longitudinal slope (m/m)
 208 n = the Manning’s roughness coefficient
 209

210 The method proposed by Zheng, Tarborton et al. (2018) calculates cross-sectional area (A),
 211 hydraulic radius (R) and streambed slope (S) from HAND, the hydrofabric information. It
 212 necessitates a user-defined roughness as illustrated in Figure 1. This iterative process is
 213 replicated for a predetermined set of stage (Y) values.
 214



215
 216

217 **Figure 1:** Process for creating stage-discharge relationships as defined in Zheng, Tarboton, et al., (2018).
 218 (a) The catchment boundary establishes contributing cells, and the flowpath length (L) and slope (S) are
 219 then defined by the hydrofabric. (b) The HAND raster stores the elevation above the nearest river cell in
 220 the contributing area. (c) The slope raster defines the effective bed surface area of each cell dependent on
 221 the raster resolution. (d) For a defined stage (e.g., $Y=2$), inundated cells (outlined in orange across panels)
 222 are determined as those where $HAND \leq Y$. The volume and bed area of the inundated cells are then
 223 computed from (b) and (c). (e) Manning's Equation estimates a flow rate Q. (f) A collection of Y-Q
 224 relations defines an SRC.

225 As illustrated in Figure 1a, possible contributing cells (all those that are “nearest a drainage”) are
 226 selected, in this case using the NHDPlusV2 catchment. The NHDPlus VAA attributes provide
 227 the stream length (L; m) and longitudinal slope (S; m/m), and the HAND raster provides the
 228 elevation difference between each grid cell and the nearest flow path. A slope raster (1c) contains
 229 the percent slope (cellSlope) of each grid cell, which can be used to estimate the effective ground
 230 surface or bed area (BA) at a given depth (Equation 2).

$$231 \quad 232 \quad BA = cellres^2 \sqrt{1 + cellslope^2} \quad (2)$$

233 For any defined stage (Y; meters), the HAND raster can be used to identify inundated cells
 234 where the HAND value is less than Y (1d). At each of these cells, a water volume (V) can be
 235 calculated as the depth of ponded water multiplied by the cell area (Equation 3).

$$236 \quad 237 \quad 238 \quad V(y) = cellres^2 \times (Y - HAND) \quad (3)$$

239 For all inundated cells, the total bed area ($\sum BA$) and volume ($\sum V(y)$) can approximate the cross-
 240 sectional area (Equation 4), wetted perimeter (Equation 5), and hydraulic radius (Equation 6)
 241 needed in Manning's Equation (Figure 1e).

242 where:

$$243 \quad 244 \quad 245 \quad 246 \quad A(y) = \sum \frac{V(y)}{L} \quad (4)$$

$$247 \quad 248 \quad WP(y) = \sum \frac{BA(y)}{L} \quad (5)$$

$$249 \quad 250 \quad R(y) = \frac{A(y)}{WP(y)} \quad (6)$$

251 Iterating this calculation over a defined set of depths using a defined single value or stage-
 252 varying roughness yields a streamflow-depth table resembling a rating curve (Figure 1f).

253 **3.2 Estimating the Roughness Terms**

254 In various hydrology subfields, roughness is often estimated based on stream order or
 255 land cover characteristics. Models such as WRF-Hydro assign roughness as a function of
 256 Strahler stream order for overland flow calculation and Muskingum-Cunge hydrograph routing
 257 (Gochis et al., 2016a). In 2016, Li introduced the NHDPlus Inundation Modeler V4.0, which
 258 relies on a separate stream order-based approach (Li, 2016). In both lumped and distributed
 259 hydrologic models, land cover datasets are frequently used to assign roughness through

260 reclassification tables, with similar methodologies applied in dam breach analysis and other 2D
 261 hydrologic and hydraulic models (Janssen, 2016; Kalyanapu et al., 2009; Z. Liu et al., 2019).

262 Furthermore studies have demonstrated that a stage-varying composite roughness (N),
 263 based on defined in-channel and overbank regions may outperform a single roughness value
 264 (Boulomytis et al., 2017; Kubrak et al., 2019; Nguyen & Fenton, 2005). The composite approach
 265 has been shown to reduce error in hydraulic models by as much as 70% for surveyed reaches
 266 (Tuozzolo et al., 2019). Although there are multiple ways to define a composite roughness,
 267 (Tullis, 2012) found Horton's equation (Equation 7: Chow, 1959) to yield the most consistent
 268 results across disparate channel types.

$$270 \quad N = \frac{(P_{ch}(n_1)^{1.5} + P_{ob}(n_2)^{1.5})^{\frac{2}{3}}}{P_{total}^{\frac{2}{3}}} \quad (7)$$

271 Where:

272 N = composite roughness value,

273 n_1 = in-channel n

274 n_2 = overbank n

275 P_{ch} = wetted channel perimeter (m)

276 P_{ob} = wetted overbank perimeter (m)

277 P_{total} = total wetted perimeter (m).

278
 279 In locations where a USGS rating curve is available, we can determine an optimized roughness
 280 by minimizing the error between observed and simulated flows. In locations without a known
 281 rating curve, we can build on prior methodologies and assign single value and composite
 282 roughness values based on stream order or land cover. Additionally, we introduce a ML
 283 approach that leverages the VAAs of the hydrographic network to estimate roughness based on
 284 patterns found in the optimization exercise. Within these approaches, multiple variants are tested,
 285 resulting in eleven unique methods that are described below.

286 **3.2.1 Optimization**

287 Optimized roughness values aim to minimize the error between simulated and observed
 288 discharge for given depths. By fitting the roughness term alone, it is assumed (tested in 3.4) that
 289 uncertainty in other inputs (DEM and hydrofabric) are minimal. To define a single roughness for
 290 each NHDPlusV2 catchment, we solved equation 1 using a nonlinear least squares regression
 291 model (NLS) based on the Gauss-Newton algorithm with 50 maximum iterations, a convergence
 292 tolerance of $1e-09$, a lower bound of 0.01, an upper bound of 0.40, and an initial guess of 0.05 (J.
 293 M. Johnson et al., 2024; J. Michael Johnson, Coll, et al., 2022). Considering the DEM and
 294 hydrofabric data as static, the roughness value (n) is the only term in Manning's equation that can
 295 be adjusted via calibration. The lower and upper bounds were selected based on literature-driven
 296 values for reasonable floodplain roughness, with the initial guess derived from the CFIM
 297 precedent. In all cases, the NLS solver converged, and varying the initial guess had no
 298 discernible impact on the estimation in a sample of 500 basins.

299 A composite roughness was defined for each catchment by treating all cells with a
 300 HAND value of 0 as in-channel, and the remaining as out-of-channel. Both n_1 and n_2 were

301 estimated using a NLS model with bounds of (0.01 and 0.20), and (0.01 and 0.40), respectively,
 302 with an initial guess of 0.05 for each. A final constraint ensured that n_i was less than n_{i-1} in each
 303 solution. Multiple starting values were tested in a selected subset of basins with no notable
 304 differences in the results. Combined, the single value and composite optimized results provide a
 305 validation dataset used throughout this research.

306 3.2.2 Stream Order-Based Estimation

307 Previous studies (Cosgrove et al., 2020; Gochis et al., 2016b; Li, 2016) have used stream order
 308 as a proxy for roughness. We aim to evaluate how these approximation tables compare to the
 309 mean and median single value optimized derived from the USGS rating curves. Table 2 presents
 310 these values alongside those used in Li (2016) and the WRF-Hydro/National Water Model
 311 version 2.0 RouteLink file. In the National Water Model implementation of WRF-Hydro, both an
 312 in-channel roughness (n) and a compound channel roughness (n_{CC}) are associated with each
 313 flowline feature of NHDPlus.

314
 315 **Table 1.** Roughness values used for the Stream order approximations

Order	Mean Optimized	Median Optimized	Li-Assignment	WRF-Hydro n	WRF-Hydro n_{CC}
<i>Source</i>			<i>Li (2016)</i>	<i>Gochis (2016)</i>	<i>Gochis (2016)</i>
1	0.196	0.187	0.14	0.060	0.12
2	0.181	0.169	0.12	0.060	0.12
3	0.157	0.134	0.09	0.055	0.11
4	0.128	0.103	0.09	0.055	0.11
5	0.107	0.079	0.07	0.050	0.10
6	0.088	0.057	0.06	0.050	0.10
7	0.083	0.051	0.03	0.045	0.09
8	0.067	0.043	0.03	0.045	0.09
9	0.047	0.029	0.03	0.040	0.08
10	0.043	0.037	0.03	0.040	0.08

316

317 3.2.3 Land Cover Estimation

318 Land cover information can provide a spatially heterogeneous perspective of the
 319 landscape, yet it is prone to sampling and resampling error as well as scale-related classification
 320 uncertainties (J Michael Johnson & Clarke, 2021; Kim et al., 2024). Foster and Maxwell (2019)
 321 identified that vegetation-defined heterogeneity influenced behavior and determined n values in
 322 the stream network, but grid resolution did not reveal a clear scaling relationship. Hence, we are
 323 interested in both single flood plain values, akin to those used in flood mapping studies,
 324 and stage-varying roughness values.

325 The 2019 National Land Cover Database (NLCD) underwent reclassification using
 326 roughness values proposed by Kalyanapu et al. (2009) and extended by Liu et al. (2019). A
 327 single floodplain roughness was calculated for each reach by averaging all cells submerged by
 328 the maximum stage in the rating curve. Furthermore, a stage-varying roughness was generated
 329 by calculating the average land cover roughness using only the inundated cells at each stage.

330

331 3.2.4 Hydrofabric Gradient Boosted Machines (GBM)

332 Roughness is dependent on a variety of channel characteristics, making it a suitable
 333 candidate for exploration with predictive ML models. After evaluating multiple options, a
 334 Gradient Boosted Machine (GBM) algorithm was selected. GBMs are known to enhance model
 335 generalizability (Friedman, 2001) but due to lack of inherent regularization, and highly complex
 336 decision boundaries they tend to focus on difficult-to-fit data points and result in overfitting.
 337 However, adjusting its hyperparameters and applying early stopping can mitigate this issue. In
 338 contrast to supervised single predictive models or those based on ensemble averages (e.g.,
 339 random forests), GBMs sequentially add new models to an ensemble and update a trained base
 340 learner with each iteration.

341 Fitting GBMs necessitates several hyperparameters, including the number of trees (T); an
 342 interaction depth (K); a learning rate (λ); and subsampling controls (p). The interaction depth
 343 (K) determines the number of splits in each tree and the pace at which the algorithm proceeds
 344 down the gradient descent. Smaller learning rates (λ) reduce the likelihood of overfitting but
 345 prolong the convergence time. While these parameters confer flexibility to GBM models, they
 346 demand intensive tuning to select appropriate values. Hence, a grid of potential hyperparameters
 347 for this problem was defined as follows (Equation 8):
 348
 349

$$350 \text{ hyperparameters} = \left\{ \begin{array}{l} k = 1, 2, \dots, 15 \\ T = 500, 1000, \dots, 5000 \dots 10000, 15000, \dots, 40000 \\ \lambda = 0.001, 0.005, 0.01, \dots, 0.1 \\ R = 5, 10, 15 \\ p = 0.3 \end{array} \right\} \quad (8)$$

351 To identify the variables that most accurately predict roughness, we defined a training dataset
 352 using a stratified random sampling method, selecting 500 or 80% of the gauged locations from
 353 each HUC2 from the Watershed Boundary Dataset. Developing a GBM approach involves a
 354 three-step process.

355 *Step 1:*

356 Initially, a series of 16,065 GBMs were fitted for each hyperparameter combination (Equation 8),
 357 using all numeric variables from the NHDPlusV2 VAA as predictors. For each model,
 358 the relative influence of each predictor was computed in addition to the number of times it was
 359 selected for splitting, weighted by the squared improvement provided at each split. These results
 360 were averaged over all trees (Friedman, 2001), and those with the highest relative influence were
 361 paired with a subjective evaluation of how easily they could be computed for general hydrofabric
 362 networks, yielding the final set of 5 core predictors:
 363

- 364 i. **Drainage Area:** Drainage area (km²) of the single flowpath catchment
- 365 ii. **Flowpath Length:** Flowline length in kilometers
- 366 iii. **Arbolate Sum:** The cumulative length of the upstream drainage network (mainstem and
 367 tributaries) from the outlet of the catchment
- 368 iv. **Path Length:** The distance from the flowline outlet to the end of the network along the
 369 mainstem path
- 370 v. **Slope:** A unitless fraction (cm/cm) of the flow path slope derived from the 30m NED

371 **Step 2:**

372 Using only these five predictors, a new set of 16,065 GBMs was trained for all hyperparameter
 373 combinations, and the combination producing the minimal RMSE was selected to train a final
 374 model. That model used the following:

- 375
 376 i. $k = 12$
 377 ii. $T = 40,000$
 378 iii. $\lambda = 0.025$
 379 iv. $R = 10$
 380 v. $p = 0.3$

381 Upon completion, the predicted roughness values generated with this model had an RMSE of
 382 0.045, and a nRMSE of 26.4%, when compared to the single value optimized roughness values.

383 **Step 3:**

384 Using the model trained in step 2, we predicted roughness across the NHDPlusV2 network.
 385 Similarly, any river segment with a known drainage area, flowpath length, arbolate sum, path
 386 length, and slope can serve as input to develop a predicted single value roughness. It is critical to
 387 note that the predicted values are unique to the input NHDPlusV2 dataset; extrapolation or
 388 conflation to a different network would likely provide poor results. Nonetheless, new data can
 389 be generated from the model provided a network topology is known

390 **3.3 Synthetic Rating Curve Comparison**

391 This optimized roughness (n), a standard default value (0.05), a stream order based, land cover
 392 based, and GBM approaches produce eleven synthetic (and one observed) rating curve at each of
 393 the 7, 270 gauged locations. For clarity, these methods are summarized in Table 2.

394

395 **Table 2:** Methods and approaches for assigning roughness for rating curves

#	Category	Name	Description
1	observed	USGS	25 evenly distributed Q-Y points built from a cubic spline fit to the observed USGS rating curve
2	default	global-roughness	Roughness of 0.05 assigned to all reaches
3	optimized	single-value	Single roughness, fit to the observed rating curve using a non-linear solver with a lower and upper bound of 0.01 and 0.4.
4	optimized	composite	Composite roughness using Horton's method where n_1 and n_2 were fit to the observed rating curve using a non-linear solver with a lower and upper bound of {0.01, 0.01} and {0.2, 0.4}.
5	stream order	Li-assignment	Roughness assigned by stream order based on Li, 2016
6	stream order	wrf-N	Roughness assigned by stream order from the 'Manning's roughness' (n) in the NWM v2.1 RouteLink file
7	stream order	wrf-Ncc	Roughness assigned by stream order from the 'Compound Channel Manning's n ' (n_{CC}) in the NWM v2.0 RouteLink file
8	stream order	mean-optimized	Roughness assigned by stream order based on mean values from the calibrated method
9	stream order	median-optimized	Roughness assigned by stream order based on median values from the calibrated method

10	land cover	single-value	Single value assigned via a reclassified land cover map using those values submerged by maximum RC stage
11	land cover	stage-varying	Stage varying values assigned via a reclassified land cover map using cells submerged by the current RC stage
12	hydrofabric	GBM	Values assigned based on output of trained GBM model using the NHDPlus VAA attributes as predictor variables

396
397
398
399
400

To assess SRC accuracy, the simulated discharge values produced with each roughness, using the USGS rating curve stage values, were compared to the USGS discharge values using the root mean squared error normalized to the mean of observed discharge (nRMSE; see Equation 9).

$$401 \quad nRMSE = 100 \times \sqrt{\frac{(Q_{src} - Q_{obs})^2}{Q_{obs}}} \quad (9)$$

402
403
404
405
406

where:

Q_{obs} = observed discharge

Q_{src} = simulated discharge.

407
408
409
410
411
412

nRMSE was calculated for the entire rating curve as well as the lower, middle, and upper sections. While defining “good” and “bad” nRMSE is subjective, a cut off of 30% nRMSE has been used to determine whether a site displays reasonable performance in prior research (Gleason & Smith, 2014; Yoon et al., 2016). For readability throughout the text, we adopt this shorthand and describe errors of 30% or less as reasonable, and errors of 100% or more as extreme.

413

3.4 Parameter Sensitivity

414
415
416
417
418

One open question about SRCs is how sensitive the results are to input data including the DEM, hydrofabric, and roughness. To decompose the SRC into its primary components, Manning’s Equation can be rewritten by substituting equations 4, 5, 6 into equation 1, and rearranging such that:

$$419 \quad Q(y) = V \times \frac{1}{n} \times \frac{1}{L} \times \sqrt{S} \quad (10)$$

420
421

Where

$$422 \quad V = \frac{Vol(y)^{\frac{5}{3}}}{BA(y)^{\frac{2}{3}}}$$

423
424
425
426
427
428
429
430
431

To understand the role of each of the input dataset in streamflow estimation, we want to perform sensitivity analyses with respect to the four uncertain parameters - V , n , L , and S - by implementing a separate sensitivity analysis at stages 1, 2, 3 ... 25 using a factorial design.

To build the factorial design for sensitivity analysis, we need to establish reasonable range bands for each of these variables that are adjustable to each site. The volume factors are driven by the DEM which is most easily influenced by the vertical accuracy as highlighted in case studies leveraging LIDAR (Zheng et al., 2018). The 10m NED has a documented vertical accuracy of 3.04 meters (Gesch et al., 2014) so we elected a test set of 0.5, 1 and 2 meters in the

432 positive and negative directions basin wide. These were implemented by adjusting the HAND
433 values throughout a given catchment prior to estimating volume and bed area.

434 To test roughness, we allow roughness to range from 0%, 10%, 25%, 50%, 100% and
435 200% error from the optimized single-value estimates while enforcing the lower and upper limits
436 of 0.01 and 0.40. Length is a byproduct of the hydrofabric resolution and higher resolution data
437 inputs like the NHD High-Resolution will likely increase reach length as more detail is captured.
438 Following research aligning multi-scalar flowline data from the EPA River Reach, Medium
439 Resolution NHDPlus and High Resolution NHD through the identification of common
440 mainstems (D. Blodgett et al., 2020), a high-level comparison revealed a range of variability
441 which we reduced to 0%, 5%, 10% and 15% percent of the NHDPlusV2 flowline values in the
442 positive and negative direction.

443 Slope is a product of the hydrofabric and underlying DEM. While the HAND and Slope
444 rasters are based on the 10m NED, the NHDPlus flowline slope is an attribute derived from the
445 30m NED. A random sample of 100 flowlines from this study were used to extract transects
446 from the 10m NED. The difference between the smoothed slopes of these transects (5 point
447 rolling mean) and the listed slope attributes of the NHDPlus were represented as a 0%, 25%,
448 50% and 75% error in each direction of the recorded values.

449 Using these possible variations, 363 randomly sampled sites were evaluated to ensure
450 accuracy at the 95% confidence level. The results of the design were analyzed with an Analysis
451 of Variance (ANOVA) method to deduce the main effects and two factor interactions using the
452 *multisensi* R package (Bidot et al., 2018). Upon completion, the results were averaged across
453 locations.

454 **4 Results**

455 A total of 81,070 synthetic rating curves (SRCs) were computed for comparison. Section
456 4.1 describes the performance of each roughness method, section 4.2 addresses errors exhibited
457 in each section of the rating curve, section 4.3 addresses the skill of the GBM model, and section
458 4.4 looks at the sensitivity of the SRCs to the roughness, DEM, and hydrofabric inputs used in
459 Manning's equation.

460 **4.1 Synthetic Rating Curve Performance Analysis**

461 Figure 2A illustrates the percentage of locations achieving reasonable and extreme error
462 for each roughness method, alongside the Spearman Correlation compared to the optimized
463 single value roughness. In the outlined section of the table, the 25th, 50th, and 75th quartile (Q1,
464 Q2, Q3) nRMSE for the complete rating curve, and the mean nRMSE for each section of the
465 rating curve are displayed. These statistics are derived solely from sites producing nRMSE <
466 100% for that method.

467 The two optimized approaches provide the least error across all metrics but are confined
468 to gaged locations. SRCs generated with an optimized composite roughness offer marginal
469 improvement over those with an optimized single value, and occasionally exhibit degraded
470 performance. This implies that a composite view, particularly when considering locations where
471 HAND = 0 as in channel, is not critical to SRC roughness estimation. The optimized single value
472 approach achieved reasonable error in ~80% of the tested locations, suggesting models
473 potential accuracy across a broad spectrum of locations. Nonetheless, the remaining 20%
474 highlight areas where the HAND-based SRC model may be incomplete or other sources of
475 uncertainty contribute to the error.

476 Amongst methods extendable to ungaged basins, the GBM method demonstrates superior
477 results and notably reduced error compared to stream order and land cover approaches. Notably,
478 it generates nearly four times as many SRCs with reasonable error as other nonsite optimized
479 methods. The correlation with the optimized single value is also double compared to the next
480 closest method.

481 All four stream order methods exhibit similar performance metrics and offer marginal
482 improvement over the global default. Stream order information primarily reduces the number of
483 sites with extreme error ($nRMSE > 100\%$). This is done best by the mean optimized stream order
484 values. This performance improvement over a global default value emphasizes that roughness is
485 a local phenomenon, and the thematic assignment is too generalized to provide significant
486 performance gains. The two land cover methods demonstrate identical performance, with neither
487 land cover method offering an improvement over the stream order methods, and added
488 substantial computational burden.

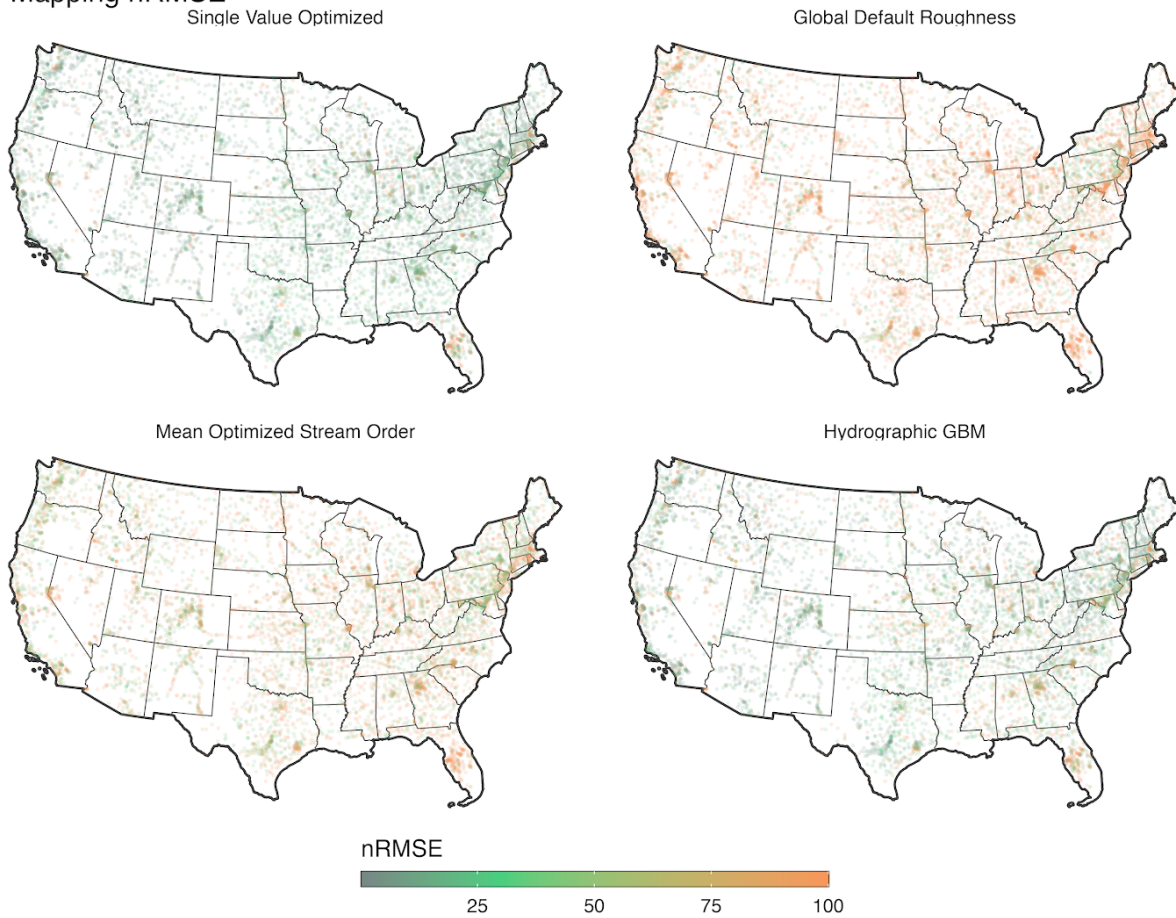
489 Finally, a default global roughness of 0.05 achieves $nRMSE \leq 30\%$ in just 10% of the
490 locations emphasizing the need for a spatially heterogeneous approach and the value in seeking a
491 more sophisticated approach. To visualize these statistical patterns spatially, Figure 2B maps the
492 $nRMSE$ from the best performing method for each approach. While the magnitudes of error in
493 the optimized and GBM methods differ, the maps highlight regions of the country where large
494 errors persist across all methods. Prominent examples include the gulf coast of Florida, the
495 eastern seaboard, the Atlanta metro region, and to a lesser extent, the lower Mississippi
496 floodplain.

497

A. Evaluation Metrics

Method	Approach	nRMSE	nRMSE	Correlation with Optimized	Q1	Q2	Q3	mean nRMSE	mean nRMSE	mean nRMSE
		≤30%	>100%		nRMSE	nRMSE	nRMSE	lower	middle	upper
Single Value	Optimized	78.10	8.81	1.00	6.14	11.88	21.58	40.22	15.79	11.73
Composite N	Optimized	76.74	10.32	NA	4.62	10.54	20.86	37.12	15.16	11.20
GBM	Hydrographic	61.85	16.21	0.88	7.46	14.76	31.38	44.70	22.40	18.61
Median Optimized	Stream Order	16.10	40.37	0.44	28.53	49.13	71.63	58.11	44.18	42.39
Mean Optimized	Stream Order	15.74	35.21	0.43	30.65	52.60	74.27	60.15	46.35	44.33
Li Assignment	Stream Order	15.09	46.29	0.41	27.74	48.10	72.06	57.90	43.83	42.08
wrf-nCC	Stream Order	14.59	40.51	0.40	30.42	51.80	73.52	59.93	46.03	43.88
wrf-n	Stream Order	12.15	59.52	0.40	25.95	46.53	73.16	56.60	43.06	42.09
Single Value	Land cover	11.50	34.74	-0.05	38.00	63.57	82.95	64.98	52.66	51.15
Stage-Varying	Land cover	11.32	34.66	NA	38.01	63.53	82.74	64.52	52.42	51.20
Global roughness	Default	11.28	61.32	NA	26.60	48.09	73.87	57.20	43.52	42.56

B. Mapping nRMSE



498
499

500 **Figure 2:** (a) Synthetic rating curve accuracy across methods. Quartile error values and the percentage of
501 sites with reasonable and extreme errors are listed. The methods are sorted by the Q2 criteria, and darker
502 hues represent better performance and are applied column-wise. (b) The nRMSE from each method is
503 mapped.

504 Across all methods, there is consistently more error in the lower section of the rating
505 curve compared to the middle and upper portions. SRCs developed with a global default and
506 mean optimized stream order have the highest mean nRMSE across all sections of the curve. The

507 single value optimized and hydrofabric GBM approaches both reduce the mean nRMSE in each
 508 section; however, the error remains higher by a factor of 2+ in the lower third. This pattern may
 509 have to do with (1) lack of bathymetric representation in HAND data for in-channel flows, (2)
 510 the datum adjustment applied to achieve a zero-flow USGS rating curve, or (3) that at smaller
 511 flows/depths, small errors are more impactful than the errors at higher flows/depths.
 512 Nonetheless, estimated SRCs demonstrate greater accuracy at the higher end of the rating curve,
 513 which holds promise for flood mapping studies and other use cases. Moreover, this staggered
 514 performance suggests the potential to optimize n for various sections of the rating curve based on
 515 flow which could be provided by the National Water Model. While a composite n was not found
 516 to be a valuable addition, a stage-varying n might offer improvements.

517 **4.2 Model and Optimized Skill**

518 The error for the single-value optimized method provides the best possible result given
 519 the current DEM, hydrofabric, and roughness bounded to the range of $\{0.01, 0.4\}$. Taking the
 520 DEM and hydrofabric data as static, the only term in Manning's equation that can be calibrated is
 521 the roughness value. The roughness value serves as a proxy for representing the ratio of water
 522 volume to discharge. Very large n values represent situations where a very strong resistance to
 523 flow is used to reduce discharge when HAND volumes are large for a given stage, but the actual
 524 SRC derived discharge is low. Very low values of n represent the opposite situation where
 525 calculated water volumes based on HAND properties are low but the required discharge is quite
 526 large. This observation may suggest a need to represent channel bathymetry to accommodate
 527 excess HAND water volumes. This section focuses on comparisons between the single optimized
 528 value and GBM approaches, particularly the cases where the imposed lower and upper limits
 529 were reached – likely to address issues in other inputs to Manning's equation.

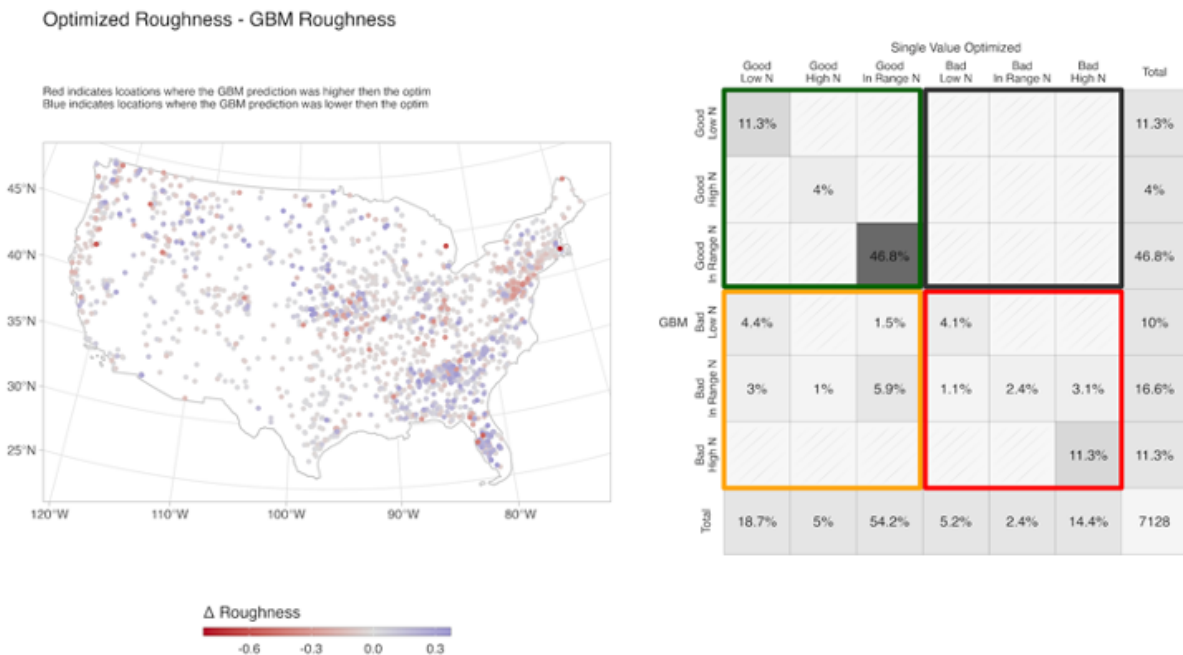
530 The error for the single-value optimized method provides the best possible result given
 531 the current DEM, hydrofabric, and roughness bounded to the range of $\{0.01, 0.4\}$. Figure 3A
 532 shows the difference in roughness between the optimized and GBM approach. Sites with an
 533 absolute value of $\Delta N < 0.01$ have been removed from the map. In this Figure, sites that appear
 534 red indicate that the N value of the GBM based on network attributes is greater than the
 535 optimized n value; conversely, sites that are blue indicate the opposite. On the East coast, we
 536 observe a landscape where the GBM tends to show greater roughness compared to the optimized
 537 values while in the southeast, the GBM tends to show lower N . The rest of the country indicates
 538 a more mixed approach, with a slight tendency for the GBM to predict n lower than the
 539 optimized approach (blue).

540 Next, we categorized the *skill* of the rating curve (by the nRMSE $< 30\%$ threshold) and
 541 whether the roughness pushed toward the upper limit (>0.35), the lower limit (<0.05), or was
 542 within a fair range ($0.05 \leq n \leq 0.35$). In total, this yielded six categories that were used to classify
 543 the GBM and optimized-based SRCs. Figure 3B shows the confusion matrix of these divided
 544 into four color-coded quadrants while Figure 3C shows categorical classification. The first
 545 column (green and orange box) represents the total number of sites that were well-served by the
 546 site-by-site optimization. In total, 77.9% of the locations achieved reasonable error, and 54.2%
 547 did so without stretching the roughness value toward the imposed limits. For those that did push
 548 roughness towards an imposed limit, the bulk stretched towards the low value. This highlights
 549 the tendency of the GBM model to favor lower roughness and a broader notion that HAND
 550 volumes tend to under-predict the actual volume flowing through the river channel. The first row
 551 (green and black box) represents the total number of sites that were well-served by the GBM

552 model. In total, 62.1% of the sites were able to achieve reasonable error, with ~15% stretching
553 the roughness value toward the imposed limits.

554 Starting in the upper left, the green section shows that 62.1% of sites achieve a
555 reasonable nRMSE in both the single-value optimization and GBM. 46.8% of these did so with
556 an in-range roughness, while ~15% pushed the upper and lower limits. Specifically, there is a
557 strong preference to push the optimization roughness towards the lower limit of 0.01. Moving
558 counterclockwise, the black box is empty, highlighting that the GBM cannot find solutions
559 where the optimization failed. The red box represents situations where both the optimization and
560 GBM methods were unable to find a solution. The implicit concern is that the errors in the input
561 data are larger than what roughness adjustments alone can correct in ~22% of the tested
562 locations.

563 In total, 17.8% of sites produced bad optimizations with the same pattern for both site-
564 based optimized and GBM methods. For example if a site had a bad nRMSE with a low n, the
565 GBM produced the same which is encouraging for the skill of the GBM, but suggests future
566 work might look to eliminate these sites in the model training. In the remaining 4.2% percent, the
567 GBM took on a low or high optimized n, and brought it into the expected range without
568 improving the performance.



Percent of sites per stream order that fall into each classification

Single Site Optimized Approach

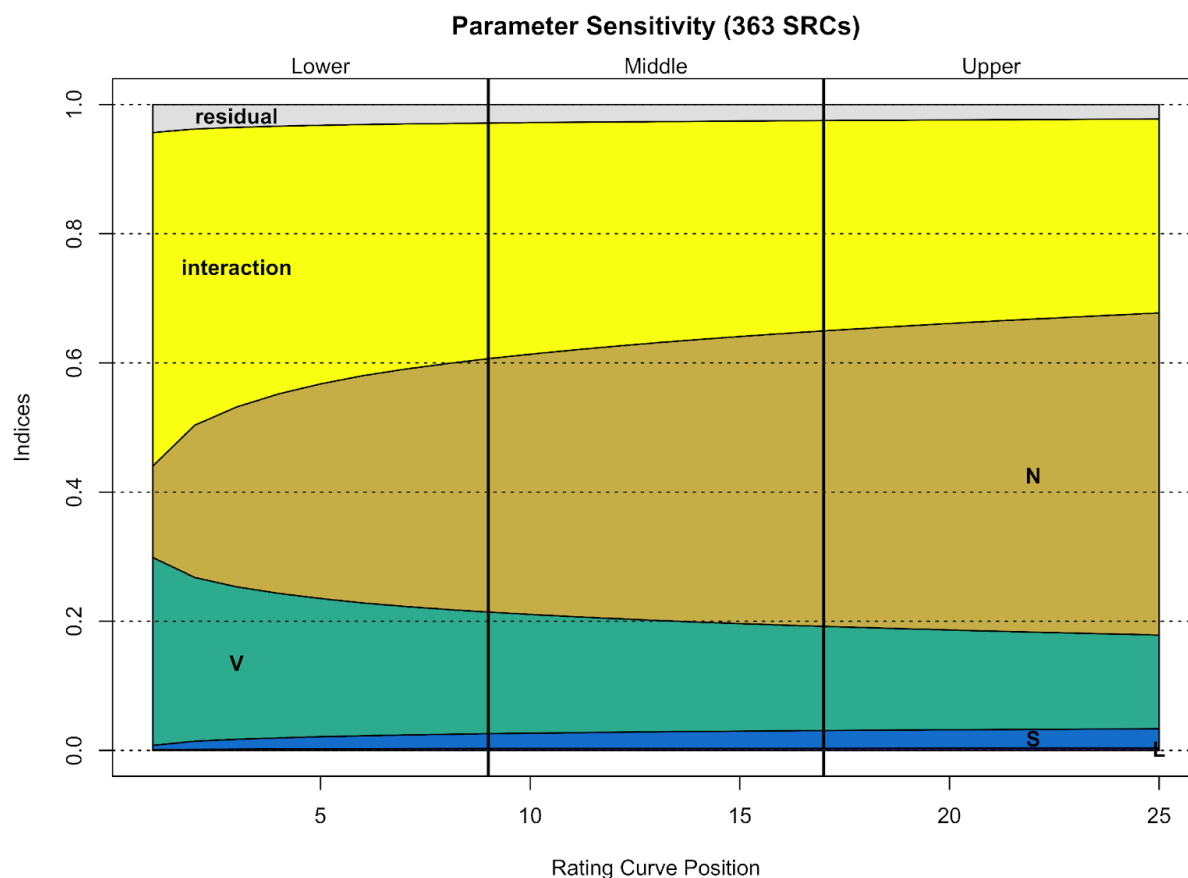
	Order 1	Order 2	Order 3	Order 4	Order 5	Order 6	Order 7	Order 8	Order 9	Order 10
Good High N	6.8	8.8	8.6	5.4	3.4	2.6	3.0	0.0	0	0
Bad High N	56.8	33.3	17.2	9.7	6.5	4.8	5.7	6.0	4	0
Good Low N	2.4	3.9	8.6	16.2	25.8	35.6	38.3	40.5	40	50
Bad Low N	0.5	1.3	1.3	3.4	7.6	10.6	10.5	21.4	24	0
Good In Range N	31.2	50.5	61.1	62.6	54.2	44.2	39.2	31.0	28	50
Bad In Range N	2.4	2.2	3.2	2.7	2.5	2.1	3.3	1.2	4	0

569
570
571 **Figure 3:** (a) The difference in roughness produced by the GBM and Optimized roughness values are
572 mapped. Red (negative values) indicate locations where the GBM prediction produces higher values than
573 the optimized approach. Blue (positive values) indicate locations where the GBM prediction produces
574 roughness lower than the optimized approach. Sites where the difference was less than ± 0.01 were
575 excluded (b) The GBM and single site optimized results were categorized by the skill of the rating curve
576 (by the nRMSE < 30% threshold), and whether the roughness pushed toward the upper limit (>0.35), the
577 lower limit (<0.05), or was within the range ($0.05 \leq N \leq 0.35$). (c) The percent of sites, per stream order,
578 that fall into each classification. Darker hues represent larger percentages. The horizontal line after order
579 4 represented a break in SRC creation performance identified in prior research.

580 **4.3 Parameter Sensitivity**

581 In this section we investigate the sensitivity of SRCs to the primary inputs using factorial
582 design and ANOVA decomposition, which include the (1) DEM, (2) hydrofabric, and (3)

583 roughness. Figure 4 shows the sensitivity indices of the main effects and first-order interactions
 584 at each point in the rating curve normalized to 1.



585
 586 **Figure 4:** Evolution of the main effects and the first-order interaction sensitivity indices of the SRC
 587 variables averaged over 363 randomly selected locations.

588 In the lower third of the rating curve, there is more sensitivity to the DEM (V), interaction terms,
 589 and residual effects. This suggests that SRCs perform worse in the lower third of the rating curve
 590 largely because they are more easily influenced by multiple factors. Starting around the middle
 591 of the rating curve, proportional sensitivity starts to stabilize with ~15% being contributed by the
 592 DEM, ~45% by roughness, and ~30% from variable interaction. There is minimal error (in total
 593 ~10%) contributed from the length, slope, or residual effects of the model combined. It is notable
 594 that as one approaches the upper end of the curve, the contribution of error from the interaction
 595 and V terms decrease further and are generally overtaken by sensitivity to roughness.

596 These results indicate that the primary challenge in developing accurate SRCs is
 597 Manning's roughness for mid and high SRC values, and very low SRCs are affected by DEM
 598 errors and missing bathymetry, but there are other key sources of uncertainty. The overwhelming
 599 sensitivity to roughness means that areas suffering from other inputs can only be identified when
 600 the uncertainty in roughness is minimized. Given that the primary objective of many operational
 601 flood inundation forecasting systems is to warn of high magnitude events, optimization of
 602 roughness for this objective seems practical. For those seeking predictive skill for lower

603 magnitude events, i.e., “nuisance” flooding, improving accuracy of base information such as the
604 DEM seems to be more critical.

605 Aside from roughness and the interaction of all inputs, the volume of water computed
606 from the DEM was the largest source of error. As the USGS 3D elevation program moves their
607 elevation program towards the collection of nationally comprehensive and complete LIDAR
608 coverage, it is worth mentioning here the possible opportunities and limitations with the method
609 provided here.

610 **5 Discussion**

611 A challenging aspect of the transferability of our proposed methodology is the scale-
612 dependency of both DEM that plays a crucial role in generating water volume for a given depth
613 defined by a HAND product, and hydrographic properties that are used for roughness
614 calculations. Ideally we would like the trained roughness ML model to be transferable to any
615 other hydrographic network generated at different scales. We conjecture that this holds true for
616 networks of comparable scale (i.e., 1:100,000 ratio). Another question is whether the assumption
617 that the variable selected during the feature importance analysis remains consistent as
618 hydrographic network scale changes? For instance in higher resolution networks, characterized
619 by the prevalence of more tributaries with greater sinuosity, the arbolate sum, a key
620 characteristic, typically demonstrates a notable increase. Consequently, if a smaller river system
621 within the higher resolution network is trained solely on lower resolution data, it might
622 erroneously exhibit attributes akin to those of a much larger system, potentially resulting in
623 artificially low roughness values.

624 Similar to hydrographic scale impact on roughness, the higher resolution LiDAR or DEM
625 data improves accuracy in channel volume estimation and synthetic rating curve calculation by
626 providing detailed terrain data, enhancing channel morphology representation, and minimizing
627 uncertainties in channel geometry and hydraulic modeling. This contributes to more reliable
628 assessments of water resources and flood risks. The utilization of LiDAR data holds promise for
629 mitigating uncertainty in volume estimations through several mechanisms. The first method, akin
630 to that employed in GeoFlood, involves increasing the horizontal (grid) resolution to yield more
631 effective “cells.” This reduction in resampling inherently enhances the vertical accuracy at each
632 cell. The second method entails utilizing LiDAR to refine vertical accuracy within the same 10m
633 grid as the current 3DEP 10m product, effectively integrating the latest data captures to enhance
634 the existing grid. In both scenarios, if a new DEM is utilized, recalibration of the base inputs to a
635 Synthetic Rating Curve (SRC) – namely, the cross-sectional area and hydraulic radius at depth Y
636 – following the methodology outlined by Zheng et al. (2017) is necessary. This entails updating
637 the GBM model based on the full hyperparameter set (Step 2) but does not necessitate retraining
638 on the complete set of VAA attributes (Step 1).

639 Despite the potential enhancements to the current DEM, the issue of changing scales (cell
640 resolution) raises an open question. To qualitatively assess the transferability of GBM-produced
641 roughness values across DEM scales, we compared the reported, tuned roughness values at five
642 USGS sites examined in Zheng et al. (2018) to the GBM values. While the GBM approach
643 tended to overpredict roughness compared to the reported GeoFlood values, a correlation was
644 observed (albeit from a limited dataset). This trend aligns with the notion that larger grid cells
645 yield larger volumes and, per equation 11, necessitate larger roughness values. The idea that
646 roughness varies with DEM resolution finds support in hydrologic modeling research. For
647 example, it has been established that 2D flood models are sensitive to DEM resolution (Fewtrell

648 et al., 2008; Horritt & Bates, 2002; Saksena & Merwade, 2015; Schumann et al., 2007), and
649 roughness (Lim et al., 2016; Mason et al., 2003; Pappenberger et al., 2005). However, conflicting
650 findings exist regarding the existence of a scaling relationship, with some studies suggesting
651 otherwise (M. Foster & M. Maxwell, 2019). Hence, it is acknowledged that the dependency of
652 GBM roughness values on DEM and hydrography constitutes a limitation of the dataset
653 produced herein, not the methodology. Future investigations will explore methods for
654 operationalizing roughness model fitting and prediction based on the methods and data (USGS
655 rating curves) developed in this study.

656 An assessment of the sites exhibiting extreme error in SRC with the calibrated n values
657 demonstrated that SRC extreme error often occurs when roughness approaches one of the
658 enforced physical limits. It was also in these areas where the largest divergence between the
659 predicted and calibrated n values was observed. In many ways, this divergence in n values offers
660 a signal for when other aspects of the SRC creation are uncharacteristically influential. The value
661 of n serves as a proxy for representing the ratio of water volume to discharge. Very large n
662 values represent situations where a very strong resistance to flow is used to reduce discharge
663 when HAND volumes are large for a given stage, but the actual SRC derived discharge is low.
664 Very low values of n represent the opposite situation where calculated water volumes based on
665 HAND properties are low but the required discharge is quite large. (perhaps suggesting a need
666 for representing channel bathymetry to accommodate excess HAND water volumes).

667 Finally, several critical considerations arise when utilizing this dataset or extending the
668 workflow beyond its current scope. The workflow, beginning with a mechanical measurement of
669 roughness to train a predictive model based on network attributes, subsequently utilized the same
670 network and DEM to establish a relationship between water surface height and discharge
671 required for that stage. However, the applicability of these findings to variations in input
672 parameters, such as alterations to the underlying network, remains unclear. Further inquiry is
673 warranted to determine whether the values derived from this dataset could be used as a direct
674 crosswalk to the new network, whether the values would need to be recalculated based on the
675 new attributes of the network using the existing model, whether the model would need retraining
676 using the new inputs, or whether the process of determining the selected features needs to be
677 performed.

678 **6 Conclusions**

679 At the onset of this research, the necessity for improved reach-level roughness was
680 highlighted to support continental flood mapping efforts. We employed the methodology
681 proposed by Zheng et al. (2017) to define reach-averaged hydraulic traits from a 10m HAND
682 product in catchments with a USGS gauge and calibrated a roughness value to minimize the
683 error in predicted flows. This approach resulted in 78% of gaged locations achieving $nRMSE \leq$
684 30%. To produce SRCs in ungauged basins, we evaluated a range of methods for estimating
685 reach-level roughness. Among these, a data-driven ML model based on NHDPlus hydrographic
686 topology proved the most robust. The ML model produced almost four times the number of
687 SRCs with acceptable error compared to non-optimizable methods (e.g., stream order and land
688 cover methods). Additionally, its correlation with the optimized single value is twice that of the
689 next closest method. The predictions were able to achieve a ranked correlation of 0.89 with the
690 optimized values and SRCs with reasonable error in 62% of the tested locations. In contrast, a
691 widely used global roughness value captured just 13% of SRCs with reasonable error, and the
692 best performing stream order parameterization captured just 16%.

693 A sensitivity test showed that the DEM and roughness are the principal sources of error
694 in the conceptual rating curve model, while length and slope are practically non-significant. We
695 demonstrated that as the upper end of the SRC is approached, it becomes apparent that the
696 contribution of error from the interaction and V terms decrease further and are generally
697 overtaken by sensitivity of roughness. These conclusions are generally in line with other work
698 that has looked at HAND-based SRC uncertainty at individual sites (Godbout et al., 2019). The
699 conclusion is that in locations where roughness is the primary contributor of uncertainty, the data
700 driven roughness and existing data inputs can produce reasonable SRCs. In areas where the
701 DEM and hydrography introduce uncertainty, the calibrated values take on a role that was not
702 *per se* roughness, but rather a broad error-reducing scalar. Such locations were not pervasive,
703 and generally clustered around regions with large built-up extents, known engineered controls, or
704 low relief. In these areas where DEM fidelity is a primary source of SRC error, there is capacity
705 for LIDAR to be used with the methods suggested as part of the GeoFlood project (Zheng et al.,
706 2018). A drawback to using LIDAR is the availability, procurement costs, and computational
707 needs associated with creating HAND and generating inundation forecasts at large scales.
708 Fortunately, the 10m DEM seems serviceable for the majority of CONUS, and the SRC error
709 map (Figure 2) can help prioritize areas where the integration of LIDAR data might be especially
710 beneficial.

711 Future work will involve exploring several avenues to address key findings in this
712 research and potential implications. Firstly, we demonstrated a disparity in error across different
713 sections of the rating curve, particularly higher error in the lower section compared to the middle
714 and upper portions. This signals a need to evaluate the absence of bathymetry in the model, as
715 the missing channel volume likely impacts the lower end of the rating curve. Secondly, the
716 findings suggest promising prospects for FIM methods that rely on Synthetic Rating Curves
717 (SRCs) for high flow applications. Thirdly, there is potential for optimizing the roughness
718 coefficient (n) for various sections of the rating curve. While a composite n was not found to be
719 beneficial, a stage-varying n might prove advantageous. Lastly, future research will explore how
720 this method scales across different networks, assessing its applicability and performance in
721 diverse hydrological settings. Within the United States, LIDAR may provide better discretization
722 and some additional bathymetry data. The effects of this can be tested at reaches that have both
723 LIDAR and USGS rating curves. These datasets can be effective in training a ML model and
724 gaining a better understanding of the effect of grid cells and data driven roughness on model
725 training. In essence, further research may be able to quantify how more location-attuned
726 roughness values can contribute to improved large-scale hydrologic routing and other
727 applications of reach-level roughness.

728 For regions outside the USA, official stream network data similar to the NHD are few
729 and far between. Publicly available data are often aggregated at lower spatial resolutions,
730 decreasing the ability to represent the full drainage network. However, the rapid increase in the
731 amount of crowd-sourced stream network data available through platforms like OpenStreetMap
732 offers the promise of high-resolution data that can be used for improved global reach level
733 modeling for smaller rivers. Localized high-resolution official drainage networks, crowd-sourced
734 stream network data offer the opportunity to evaluate the impact of scale, network density, and
735 attributes on the ability of GBM models to characterize the rating curve relationship. Overall, the
736 value of the current work lies in the data produced for the scale of the medium-resolution NHD
737 and 10m 3DEP product, as well as a method and curated set of training data to apply to other
738 scales within and outside the United States. The roughness values have been made publicly

739 available on HydroShare with easy-access options for both R and Python. With respect to R, the
 740 roughness values can be accessed with the nhdplusTools *get_vaa* functionalities. We hope the
 741 use of this data can support improved flood forecasting, applications that need to estimate
 742 roughness, and can prompt consideration of what other hydrologic properties and characteristics
 743 can be learned and supported by the topology implicit to hydrography datasets.

744

745 **Acknowledgments**

746 Parts of writing this work were performed with funding from the National Science Foundation's
 747 Urban Flooding Open Knowledge Network Center (Grants 1937099, 2033607). Any opinions,
 748 findings, and conclusions or recommendations expressed in this material are those of the authors
 749 and do not reflect the views of the National Science Foundation.

750

751 **Disclaimer**

752 The views expressed in this article do not necessarily represent the views of NOAA or the United
 753 States.

754

755 **Open Research**

756 The roughness values generated in the research are available at (J M Johnson, 2021). The GBM
 757 model is available at <https://github.com/LynkerIntel/hydrofabricML>. A version of this software
 758 will be published through Zenodo after the review process to accommodate for any needed
 759 changes.

760

761 **References**

- 762 Barnes, H. H. (1967). *Roughness characteristics of natural channels*. US Government Printing Office.
 763 Benson, M. A., & Dalrymple, T. (1967). *General field and office procedures for indirect discharge measurements*.
 764 US Govt. Print. Off.,.
 765 Beran, B., & Piasecki, M. (2008). Availability and coverage of hydrologic data in the US geological survey National
 766 Water Information System (NWIS) and US Environmental Protection Agency Storage and Retrieval
 767 System (STORET). *Earth Science Informatics*, 1(3–4), 119–129.
 768 Bidot, C., Lamboni, M., & Monod, H. (2018). Multisensi: Multivariate sensitivity analysis. *R Package Version*, 2,
 769 1–1.
 770 Blodgett, D., Johnson, J. M., Sondheim, M., Wieczorek, M., & Frazier, N. (2020). Mainstems: A logical data model
 771 implementing mainstem and drainage basin feature types based on WaterML2 Part 3: HY_Features
 772 concepts. *Environmental Modelling & Software*, 104927.
 773 Blodgett, D., Johnson, J. M., & Bock, A. (2023). Generating a reference flow network with improved connectivity to
 774 support durable data integration and reproducibility in the coterminous US. *Environmental Modelling &*
 775 *Software*, 165, 105726.
 776 Blodgett, D. L., & Johnson, J. M. (2022a). Hydrologic modeling and river corridor applications of HY_Features
 777 concepts. Retrieved from <http://www.opengis.net/doc/PER/22-040>
 778 Blodgett, D. L., & Johnson, J. M. (2022b). nhdplusTools: Tools for Accessing and Working with the NHDPlus.
 779 Bock, A., Blodgett, D. L., Johnson, J. M., Santiago, M., & Wieczorek, M.E. (2022). *National Hydrologic Geospatial*
 780 *Fabric Reference and Derived Hydrofabrics: U.S. Geological Survey data release*. Retrieved from
 781 <https://doi.org/10.5066/P9NFPB5S>
 782 Boulomytis, V. T. G., Zuffo, A. C., Dalfré Filho, J. G., & Imteaz, M. A. (2017). Estimation and calibration of
 783 Manning's roughness coefficients for ungaged watersheds on coastal floodplains. *International Journal of*
 784 *River Basin Management*, 15(2), 199–206.
 785 Chow, V. T. (1959). Open-channel hydraulics. *McGraw-Hill Civil Engineering Series*.
 786 Cosgrove, B. A., Gochis, D. J., Clark, E. P., & Flowers, T. (2020, January 13). NOAA's National Water Model: A
 787 Dynamically Evolving Operational Hydrologic Forecasting Framework. American Meteorological Society.
 788 Retrieved from <https://ams.confex.com/ams/2020Annual/webprogram/Paper365698.html>

- 789 Dallo, I., Stauffacher, M., & Marti, M. (2020). What defines the success of maps and additional information on a
790 multi-hazard platform? *International Journal of Disaster Risk Reduction*, 49, 101761.
- 791 De Cicco, L. A., Lorenz, D., Hirsch, R. M., Watkins, W., & Johnson, M. (2018). *dataRetrieval: R packages for*
792 *discovering and retrieving water data available from U.S. federal hydrologic web services* (manual).
793 Reston, VA: U.S. Geological Survey / U.S. Geological Survey. <https://doi.org/10.5066/P9X4L3GE>
- 794 Farmer, W. H., LaFontaine, J. H., & Hay, L. E. (2019). Calibration of the US geological survey national hydrologic
795 model in ungauged basins using statistical at-site streamflow simulations. *Journal of Hydrologic*
796 *Engineering*, 24(11), 04019049.
- 797 Fewtrell, T., Bates, P. D., Horritt, M., & Hunter, N. (2008). Evaluating the effect of scale in flood inundation
798 modelling in urban environments. *Hydrological Processes: An International Journal*, 22(26), 5107–5118.
- 799 Friedman, J. H. (2001). Greedy function approximation: a gradient boosting machine. *Annals of Statistics*, 1189–
800 1232.
- 801 Garousi-Nejad, I., Tarboton, D. G., Aboutaleb, M., & Torres-Rua, A. F. (2019). Terrain Analysis Enhancements to
802 the Height Above Nearest Drainage Flood Inundation Mapping Method. *Water Resources Research*,
803 55(10), 7983–8009. <https://doi.org/10.1029/2019WR024837>
- 804 Gesch, D. B., Oimoen, M. J., & Evans, G. A. (2014). *Accuracy assessment of the US Geological Survey National*
805 *Elevation Dataset, and comparison with other large-area elevation datasets: SRTM and ASTER* (No.
806 2331–1258). US Geological Survey.
- 807 Gleason, C. J., & Smith, L. C. (2014). Toward global mapping of river discharge using satellite images and at-many-
808 stations hydraulic geometry. *Proceedings of the National Academy of Sciences*, 111(13), 4788–4791.
- 809 Gochis, D., Dugger, A., McCreight, J., Karsten, L. R., Logan, Yu, W., et al. (2016a). *Technical Description of the*
810 *National Water Model Implementation of WRF-Hydro*.
- 811 Gochis, D., Dugger, A., McCreight, J., Karsten, L. R., Logan, Yu, W., et al. (2016b). *Technical Description of the*
812 *National Water Model Implementation of WRF-Hydro*.
- 813 Godbout, L., Zheng, J. Y., Dey, S., Eyclade, D., Maidment, D., & Passalacqua, P. (2019). Error assessment for
814 height above the nearest drainage inundation mapping. *JAWRA Journal of the American Water Resources*
815 *Association*, 55(4), 952–963.
- 816 Guerrero, J.-L., Westerberg, I. K., Halldin, S., Xu, C.-Y., & Lundin, L.-C. (2012). Temporal variability in stage–
817 discharge relationships. *Journal of Hydrology*, 446, 90–102.
- 818 Guven, A., & Aytok, A. (2009). New Approach for Stage–Discharge Relationship: Gene-Expression Programming.
819 *Journal of Hydrologic Engineering*, 14(8), 812–820. [https://doi.org/10.1061/\(ASCE\)HE.1943-](https://doi.org/10.1061/(ASCE)HE.1943-5584.0000044)
820 5584.0000044
- 821 Hamilton, A., & Moore, R. (2012). Quantifying Uncertainty in Streamflow Records. *Canadian Water Resources*
822 *Journal/Revue Canadienne Des Ressources Hydriques*, 37(1), 3–21.
- 823 Hamilton, S. (2008). Sources of uncertainty in Canadian low flow hydrometric data. *Canadian Water Resources*
824 *Journal*, 33(2), 125–136.
- 825 Horritt, M., & Bates, P. (2002). Evaluation of 1D and 2D numerical models for predicting river flood inundation.
826 *Journal of Hydrology*, 268(1–4), 87–99.
- 827 Hutton, C. J., Brazier, R. E., Nicholas, A. P., & Nearing, M. (2012). On the effects of improved cross-section
828 representation in one-dimensional flow routing models applied to ephemeral rivers. *Water Resources*
829 *Research*, 48(4), 2011WR011298. <https://doi.org/10.1029/2011WR011298>
- 830 Janssen, C. (2016). Manning’s n Values for Various Land Covers To Use for Dam Breach Analyses by NRCS in
831 Kansas. PAC.
- 832 Jarrett, R. D. (1984). Hydraulics of high-gradient streams. *Journal of Hydraulic Engineering*, 110(11), 1519–1539.
- 833 Johnson, J M. (2021). NHDPlus Value Added Attributes - no geometries. HydroShare. Retrieved from
834 <https://www.hydroshare.org/resource/6092c8a62fac45be97a09bfd0b0bf726/>
- 835 Johnson, J. M., Afshari, S., & Rad, A. M. (2024). AHGestimation: An R package for computing robust, mass
836 preserving hydraulic geometries and rating curves. *JOSS (in Review)*.
- 837 Johnson, J. Michael. (2022). National Hydrologic Geospatial Fabric (hydrofabric) for the Next Generation
838 (NextGen) Hydrologic Modeling Framework. HydroShare. Retrieved from
839 <http://www.hydroshare.org/resource/129787b468aa4d55ace7b124ed27dbde>
- 840 Johnson, J Michael, & Clarke, K. C. (2021). An area preserving method for improved categorical raster resampling.
841 *Cartography and Geographic Information Science*, 1–13.
- 842 Johnson, J Michael, Coll, J. M., Ruess, P. J., & Hastings, J. T. (2018). Challenges and Opportunities for Creating
843 Intelligent Hazard Alerts: The “FloodHippo” Prototype. *Journal of the American Water Resources*
844 *Association*.

- 845 Johnson, J Michael, Munasinghe, D., Eyelade, D., & Cohen, S. (2019). An Integrated Evaluation of the National
846 Water Model (NWM)–Height Above Nearest Drainage (HAND) Flood Mapping Methodology. *Natural*
847 *Hazards and Earth System Sciences*, 19(11), 2405–2420.
- 848 Johnson, J. Michael, Coll, J., Clarke, K. C., Afshari, S., Saksena, S., & Yeghiazarian, L. (2022). Determining
849 Feature Based Hydraulic Geometry and Rating Curves using a Physically Based, Computationally Efficient
850 Framework. Retrieved from <https://www.preprints.org/manuscript/202212.0390>
- 851 Johnson, J. Michael, Narock, T., Singh-Mohudpur, J., Fils, D., Clarke, K. C., Saksena, S., et al. (2022). Knowledge
852 graphs to support real-time flood impact evaluation. *AI Magazine*, 43(1), 40–45.
853 <https://doi.org/10.1002/aaai.12035>
- 854 Kalyanapu, A. J., Burian, S. J., & McPherson, T. N. (2009). Effect of land use-based surface roughness on
855 hydrologic model output. *Journal of Spatial Hydrology*, 9(2).
- 856 Karamouz, M., & Mahani, F. F. (2021). DEM Uncertainty Based Coastal Flood Inundation Modeling Considering
857 Water Quality Impacts. *Water Resources Management*, 35(10), 3083–3103.
858 <https://doi.org/10.1007/s11269-021-02849-9>
- 859 Kean, J. W., & Smith, J. D. (2005). Generation and verification of theoretical rating curves in the Whitewater River
860 basin, Kansas. *Journal of Geophysical Research: Earth Surface*, 110(F4).
- 861 Kean, J. W., & Smith, J. D. (2010). Calculation of stage-discharge relations for gravel bedded channels. *Journal of*
862 *Geophysical Research: Earth Surface*, 115(F3).
- 863 Kim, D.-H., Johnson, J. M., Clarke, K. C., & McMillan, H. K. (2024). Untangling the impacts of land cover
864 representation and resampling in distributed hydrological model predictions. *Environmental Modelling &*
865 *Software*, 172, 105893.
- 866 Kubrak, E., Kubrak, J., Koziol, A., Kiczko, A., & Krukowski, M. (2019). Apparent Friction Coefficient Used for
867 Flow Calculation in Straight Compound Channels. *Water*, 11(4), 745.
- 868 Li, Z. (2016, June). *A Framework of ArcGIS-Based Flood Inundation Modeling and Mapping System*,. Presented at
869 the ESRI Proceedings, ESRI Proceedings. Retrieved from
870 https://proceedings.esri.com/library/userconf/proc16/papers/265_671.pdf
- 871 Lim, N. J., Brandt, S. A., & Seipel, S. (2016). Visualisation and evaluation of flood uncertainties based on ensemble
872 modelling. *International Journal of Geographical Information Science*, 30(2), 240–262.
- 873 Limerinos, J. T. (1970). Determination of the Manning coefficient from measured bed roughness in natural
874 channels.
- 875 Liu, Y. Y., Maidment, D. R., Tarboton, D. G., Zheng, X., & Wang, S. (2018). A CyberGIS Integration and
876 Computation Framework for High-Resolution Continental-Scale Flood Inundation Mapping. *Journal of the*
877 *American Water Resources Association*.
- 878 Liu, Y. Y., Tarboton, D. G., & Maidment, D. R. (2020, June 1). Height Above Nearest Drainage (HAND) and
879 Hydraulic Property Table for CONUS - Version 0.2.1. (20200601). (Version Version 0.2.1). Oak Ridge
880 Leadership Computing Facility. Retrieved from 10.13139/ORNLNCCS/1630903
- 881 Liu, Z., Merwade, V., & Jafarzagdegan, K. (2019). Investigating the role of model structure and surface roughness in
882 generating flood inundation extents using one-and two-dimensional hydraulic models. *Journal of Flood*
883 *Risk Management*, 12(1), e12347.
- 884 M. Foster, L., & M. Maxwell, R. (2019). Sensitivity analysis of hydraulic conductivity and Manning's n parameters
885 lead to new method to scale effective hydraulic conductivity across model resolutions. *Hydrological*
886 *Processes*, 33(3), 332–349.
- 887 Maidment, D. R. (2016). Conceptual Framework for the National Flood Interoperability Experiment. *JAWRA*
888 *Journal of the American Water Resources Association*, 53(2), 245–257.
- 889 Mansanarez, V., Renard, B., Coz, J. L., Lang, M., & Darienzo, M. (2019). Shift Happens! Adjusting Stage-
890 Discharge Rating Curves to Morphological Changes at Known Times. *Water Resources Research*, 55(4),
891 2876–2899. <https://doi.org/10.1029/2018WR023389>
- 892 Marcus, W. A., Roberts, K., Harvey, L., & Tackman, G. (1992). An evaluation of methods for estimating Manning's
893 n in small mountain streams. *Mountain Research and Development*, 227–239.
- 894 Mason, D. C., Cobby, D. M., Horritt, M. S., & Bates, P. D. (2003). Floodplain friction parameterization in two-
895 dimensional river flood models using vegetation heights derived from airborne scanning laser altimetry.
896 *Hydrological Processes*, 17(9), 1711–1732.
- 897 McCormack, K. A., Levin, H. K., Morris, A. L., Fredericks, J. G., Huening, V., Tavakoly, A., et al. (2022).
898 Validation of TDX-Hydro; a global, TanDEM-X derived, 12m resolution hydrographic data suite. In *AGU*
899 *Fall Meeting Abstracts* (Vol. 2022, pp. H43B-06). Retrieved from
900 <https://ui.adsabs.harvard.edu/abs/2022AGUFM.H43B..06M/abstract>

- 901 McKay, L., Bondelid, T., Dewald, T., Johnston, J., Moore, R., & Rea, A. (2012). NHDPlus Version 2: user guide.
902 *US Environmental Protection Agency*.
- 903 McMahon, T. A., & Peel, M. C. (2019). Uncertainty in stage–discharge rating curves: application to Australian
904 Hydrologic Reference Stations data. *Hydrological Sciences Journal*, 64(3), 255–275.
- 905 McMillan, H., & Westerberg, I. (2015). Rating curve estimation under epistemic uncertainty. *Hydrological
906 Processes*, 29(7), 1873–1882.
- 907 Muste, M., Lee, K., & Bertrand-Krajewski, J.-L. (2012). Standardized uncertainty analysis for hydrometry: a review
908 of relevant approaches and implementation examples. *Hydrological Sciences Journal*, 57(4), 643–667.
- 909 Nguyen, H., & Fenton, J. (2005). Identification of roughness in compound channels (pp. 2512–2518). Presented at
910 the MODSIM 2005 international congress on modelling and simulation. Modelling and Simulation Society
911 of Australia and New Zealand.
- 912 Nobre, A. D., Cuartas, L. A., Hodnett, M., Rennó, C. D., Rodrigues, G., Silveira, A., et al. (2011). Height Above the
913 Nearest Drainage—a hydrologically relevant new terrain model. *Journal of Hydrology*, 404(1–2), 13–29.
- 914 Pappenberger, F., Beven, K., Horritt, M., & Blazkova, S. (2005). Uncertainty in the calibration of effective
915 roughness parameters in HEC-RAS using inundation and downstream level observations. *Journal of
916 Hydrology*, 302(1–4), 46–69.
- 917 Pavelsky, T. M. (2014). Using width-based rating curves from spatially discontinuous satellite imagery to monitor
918 river discharge. *Hydrological Processes*, 28(6), 3035–3040.
- 919 Qi, W., & Liu, J. (2019). Studies on changes in extreme flood peaks resulting from land-use changes need to
920 consider roughness variations. *Hydrological Sciences Journal*, 64(16), 2015–2024.
921 <https://doi.org/10.1080/02626667.2019.1669039>
- 922 Rennó, C. D., Nobre, A. D., Cuartas, L. A., Soares, J. V., Hodnett, M. G., Tomasella, J., & Waterloo, M. J. (2008).
923 HAND, a new terrain descriptor using SRTM-DEM: Mapping terra-firme rainforest environments in
924 Amazonia. *Remote Sensing of Environment*, 112(9), 3469–3481.
- 925 Rojas, M., Quintero, F., & Krajewski, W. F. (2020). Performance of the national water model in iowa using
926 independent observations. *JAWRA Journal of the American Water Resources Association*, 56(4), 568–585.
- 927 Saksena, S., & Merwade, V. (2015). Incorporating the effect of DEM resolution and accuracy for improved flood
928 inundation mapping. *Journal of Hydrology*, 530, 180–194.
- 929 Schumann, G., Matgen, P., Hoffmann, L., Hostache, R., Pappenberger, F., & Pfister, L. (2007). Deriving distributed
930 roughness values from satellite radar data for flood inundation modelling. *Journal of Hydrology*, 344(1–2),
931 96–111.
- 932 Tesfa, T. K., Tarboton, D. G., Watson, D. W., Schreuders, K. A., Baker, M. E., & Wallace, R. M. (2011). Extraction
933 of Hydrological Proximity Measures from DEMs Using Parallel Processing. *Environmental Modelling &
934 Software*, 26(12), 1696–1709.
- 935 Tullis, B. P. (2012). *Hydraulic loss coefficients for culverts* (Vol. 734). Transportation Research Board.
- 936 Tuozzolo, S., Langhorst, T., de Moraes Frasson, R. P., Pavelsky, T., Durand, M., & Schobelock, J. J. (2019). The
937 impact of reach averaging Manning’s equation for an in-situ dataset of water surface elevation, width, and
938 slope. *Journal of Hydrology*, 578, 123866.
- 939 Westerberg, I., Guerrero, J., Seibert, J., Beven, K., & Halldin, S. (2011). Stage-discharge uncertainty derived with a
940 non-stationary rating curve in the Choluteca River, Honduras. *Hydrological Processes*, 25(4), 603–613.
- 941 Yamazaki, D., Ikeshima, D., Sosa, J., Bates, P. D., Allen, G. H., & Pavelsky, T. M. (2019). MERIT Hydro: A High-
942 Resolution Global Hydrography Map Based on Latest Topography Dataset. *Water Resources Research*,
943 55(6), 5053–5073. <https://doi.org/10.1029/2019WR024873>
- 944 Yoon, Y., Beighley, E., Lee, H., Pavelsky, T., & Allen, G. (2016). Estimating flood discharges in reservoir-regulated
945 river basins by integrating synthetic SWOT satellite observations and hydrologic modeling. *Journal of
946 Hydrologic Engineering*, 21(4), 05015030.
- 947 Zheng, X., Tarboton, D. G., Maidment, D. R., Liu, Y. Y., & Passalacqua, P. (2017). River channel geometry and
948 rating curve estimation using height above the nearest drainage. *Journal of the American Water Resources
949 Association*.
- 950 Zheng, X., Maidment, D. R., Tarboton, D. G., Liu, Y. Y., & Passalacqua, P. (2018). GeoFlood: Large-Scale Flood
951 Inundation Mapping Based on High-Resolution Terrain Analysis. *Water Resources Research*.
- 952